AD-A082 346 POLYTECHNIC INST OF NEW YORK BROOKLYN DEPT OF PHYSIC--ETC F/G 11/6
CALCULATIONS OF STRESS-STRAIN RELATIONS IN ALPHA-BETA TI-MN ALL--ETC(U)
FEB 80 S ANKEM, H MARGOLIN N00014-75-C-0793

UNCLASSIFIED NL

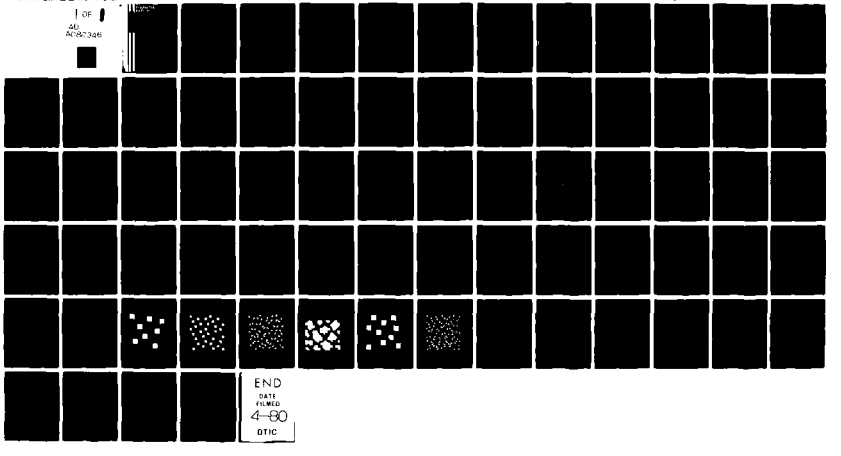

1 OF 1
AD
A082346

END
DATE FILMED
4-80
DTIC

Polytechnic Institute of New York

12

LEVEL II

CALCULATIONS OF STRESS-STRAIN RELATIONS IN ALPHA-BETA Ti-Mn ALLOYS

by

Sreeramamurthy Ankem and Harold Margolin
Department of Physical and Engineering Metallurgy
Brooklyn, New York 11201
February 5, 1980

Technical Report #2 on Contract N-00014-75-C-0793

to

Office of Naval Research
Arlington, Virginia

(9) Technical Rept. No. 2 (Annual) 1 Apr 79 - 5 Feb 80

(12)

(6) CALCULATIONS OF STRESS-STRAIN RELATIONS IN ALPHA-BETA Ti-Mn ALLOYS

by

(10) Sreeramamurthy Ankem and Harold Margolin
Department of Physical and Engineering Metallurgy
Brooklyn, New York 11201
February 5, 1980

(11) 5 Feb 80

(15) Technical Report #2 on Contract N-00014-75-C-0793

(16) 7125

to

Office of Naval Research
Arlington, Virginia

410 137

Unclassified

SECURITY CLASSIFICATION OF THIS PAGE (When Data Entered)

REPORT DOCUMENTATION PAGE		READ INSTRUCTIONS BEFORE COMPLETING FORM
1. REPORT NUMBER	2. GOVT ACCESSION NO.	3. RECIPIENT'S CATALOG NUMBER
4. TITLE (and Subtitle) Calculation of Stress-Strain Relations in Alpha-Beta Ti-Mn Alloys		5. TYPE OF REPORT & PERIOD COVERED Annual Report 1 April 1979-Feb. 5, 1980
		6. PERFORMING ORG. REPORT NUMBER Technical Report #2
7. AUTHOR(s) Sreeramamurthy Ankem and Harold Margolin		8. CONTRACT OR GRANT NUMBER(s) N 00014-75-C-0793
9. PERFORMING ORGANIZATION NAME AND ADDRESS Polytechnic Institute of New York 333 Jay Street Brooklyn, New York 11201		10. PROGRAM ELEMENT, PROJECT, TASK AREA & WORK UNIT NUMBERS Project # NR 031-779
11. CONTROLLING OFFICE NAME AND ADDRESS Office of Naval Research Arlington, Virginia		12. REPORT DATE Feb. 1980
		13. NUMBER OF PAGES
14. MONITORING AGENCY NAME & ADDRESS(if different from Controlling Office)		15. SECURITY CLASS. (of this report)
		15a. DECLASSIFICATION/DOWNGRADING SCHEDULE

16. DISTRIBUTION STATEMENT (of this Report)

Distribution Unlimited

17. DISTRIBUTION STATEMENT (of the abstract entered in Block 20, if different from Report)

18. SUPPLEMENTARY NOTES

19. KEY WORDS (Continue on reverse side if necessary and identify by block number)

Elastic stress, interface, finite element method, Widmanstatten colony, elastic interaction, elastic and plastic strain, alpha-beta titanium

20. ABSTRACT (Continue on reverse side if necessary and identify by block number)

Elastic interactions at the Widmanstatten α-β titanium alloy interfaces that arise due to compatibility requirements have been calculated for various orientations of the interface with respect to the stress axis. It is shown that maximum interactions are found when the stress axis lies in or close to the interface and 40° away from (0001)$_\alpha$.

DD FORM 1 JAN 73 1473 EDITION OF 1 NOV 65 IS OBSOLETE

SECURITY CLASSIFICATION OF THIS PAGE (When Data Entered)

β aids the elastic deformation of α much more strongly on the basal slip systems than on either prism or pyramidal slip systems. The significance of these interactions stresses on the initiation of plastic flow is considered. The effect of the interface phase on the elastic interaction stresses has been considered and a possible role of interface stresses on elevated temperature creep of α-β alloys has been suggested.

By use of a NASTRAN (18) Computer Program, the Finite Element Method (FEM) has been employed to calculate the effect of particle size, matrix and volume fraction on the stress-strain relations of α-β titanium alloys. It was found that, for a given volume fraction, the calculated stress-strain curve was higher for a finer particle size than for a coarse particle size within the range of the strains considered. This behavior was seen for all the different volume fraction alloys considered. The calculated stress-strain curves for four different vol. % α alloys were compared with their corresponding experimental curves and in general good agreement was found. Whenever there were discrepancies, they were discussed by comparing the morphology of the mesh used in the calculations with the morphology of the actual materials.

TABLE OF CONTENTS

		Page
PART-I:	The Role of Elastic Interaction Stresses on the Onset of Plastic Flow for Oriented Two Ductile Phase Structures	
I.	Introduction	1
II.	Theoretical Considerations	2
III.	Procedure	4
IV.	Results	8
V.	Discussion	10
VI.	Summary	18
VII.	Acknowledgements	19
VIII.	References	20
IX.	Figures	22
X.	Tables	23
PART-II:	Finite Element Method (FEM) Calculations of Stress-Strain Behavior of Alpha-Beta Ti-Mn Alloys	33
I.	Procedure	36
II.	Results and Discussion	40
III.	Conclusions	46
IV.	Acknowledgements	47
V.	References	48
VI.	Figures	49

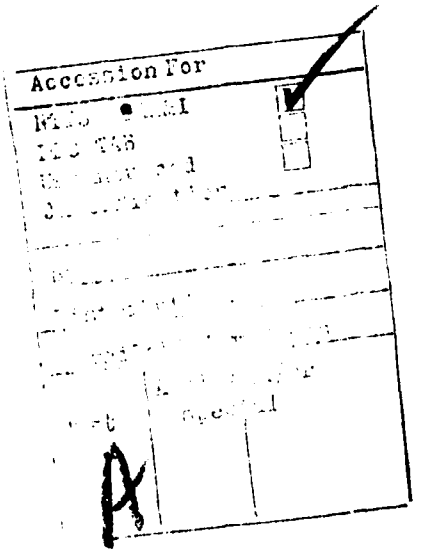

PREFACE

This report is written with two independent parts, which are entirely self contained.

Part I. is the Role of Elastic Interaction Stresses on the Onset of Plastic Flow for Oriented two Phase Structures.

Part II. is the Finite Element Method (FEM) Calculations of Stress Strain Behavior of Alpha-Beta Ti-Mn Alloys.

PART-I: THE ROLE OF ELASTIC INTERACTION STRESSES ON THE ONSET OF PLASTIC FLOW FOR ORIENTED TWO DUCTILE PHASE STRUCTURES

ABSTRACT

Elastic interactions at the Widmanstätten α-β titanium alloy interfaces that arise due to compatability requirements have been calculated for various orientations of the interface with respect to the stress axis. It is shown that maximum interactions are found when the stress axis lies in or close to the interface and 40° away from $[0001]_{\alpha}$. The interaction stresses could be of the order of 30-35 percent of the resolved shear stress on the basal slip systems. β aids the elastic deformation of α much more strongly on the basal slip systems than on either prism or pyramidal slip systems. The significance of these interactions stresses on the initiation of plastic flow is considered and it is shown that a good qualitative agreement has been obtained between these calculations and an earlier investigation by Wojcik and Koss (24). The effect of the interface phase on the elastic interaction stresses has been considered and a possible role of interface stresses on elevated temperature creep of α - β alloys has been suggested.

INTRODUCTION

Increasing interest is developing in the role of colonies of Widmanstätten α in the deformation behaviour of α-β alloys. In this paper we examine the conditions leading to general slip across a colony of Widmanstätten α surrounded by β.

Slip traversing many Widmanstätten platelets in a colony in various α-β titanium alloys has been observed by several investigators including Wells and Sullivan(1), Greenfield and Mangolin (2), Eylon et. al (3), Eylon and Hall (4), Shechtman and Eylon (5), and Eylon and Bania (6). Since α precipitates in the β with the Burgers orientation relationship (7)

$$(000\,1)_\alpha \;//\; \{110\}_\beta$$

$$\langle 11\bar{2}0\rangle_\alpha \;//\; \langle 111\rangle_\beta$$

and from which it follows

$$\{0\,\bar{1}\,10\}_\alpha \;//\; \{1\,\bar{1}\,2\}_\beta$$

$$\langle 11\,\bar{2}0\rangle_\alpha \;//\; \langle 111\rangle_\beta$$

and

$$\{01\,\bar{1}\,1\}_\alpha \;//\; \{\bar{1}01\,\bar{1}\}_\beta$$

$$\langle 11\,\bar{2}0\rangle_\alpha \;//\; \langle 111\rangle_\beta$$

It is expected that slip transfer would be easy for these Burger's oriented slip systems. However, this orientation relationship does not explain what is the effect of the elastic and elastic-plastic compatability stresses at the α-β interface on the slip in α and β and across the colony. It will be shown later that long range elastic interaction stresses exist at the α-β interfaces and certainly would effect the slip behavior in and across α and β. The effect of the interface phase (8, 9, 10), that may exist in some of the

titanium alloys, on the slip behavior is also considered and will be discussed.

THEORETICAL CONSIDERATIONS

Hook and Hirth (11) have shown that elastic interaction stresses at the grain boundaries of bicrystals give rise to local stresses which result in the operation of secondary slip systems not normally expected to function in the individual single crystal components. Similar behaviour has also been reported on β-brass bicrystal (12) and β-brass bicrystal and tricrystal (13). These observations can be looked at in a different sense, i.e. the interaction stresses may oppose slip in some slip systems and aid it in other slip systems.

If one assumes a cartesian coordinate system xyz such that x and z axis lie in the plane of the two phase α-β interface (Fig. 1). Then the continuity of strain across the interface is related by

$$e^{\alpha}_{xx} = e^{\beta}_{xx},\quad e^{\alpha}_{zz} = e^{\beta}_{zz},\quad e^{\alpha}_{zx} = e^{\beta}_{zx} \qquad (1)$$

The other strain components may be important in considering the effects of end constraints but do not affect the deformation of an arbitrary boundary (11). It is possible to resolve the elastic compatibility strains of eqs[1] individually onto a given slip system and add them to determine the magnitude of the resolved elastic strain in this slip system. For a parallel slip system in α and β and since eqs [1] apply

$$e^{\alpha}_{t} = e^{\beta}_{t} \qquad [2]$$

where e^{α}_{t} and e^{β}_{t} are the total resolved shear strains from eqs [1] of α and β respectively.

Let us consider that this common slip system is a primary slip system

of α and β. Let the slip plane in each phase be the yz plane and the slip directions be z, Fig. 1. The orientation of this slip direction is not the Burgers orientation, because for this specific orientation the slip direction is not parallel to the interface as Fig. 2 indicates.

The equations relating eqs[1] and[2] as follows

$$\left.\begin{aligned} e_t^{\alpha} &= 2e^{\alpha}_{xx} \cos o_1 \cos \lambda_1 + 2e^{\alpha}_{zz} \cos o_3 \cos \lambda_3 + e^{\alpha}_{zx} (\cos \phi_3 \\ &\cos \lambda_1 + \cos \phi_1 \cos \lambda_3) \\ e_t^{\beta} &= 2e^{\beta}_{xx} \cos \phi_1 \cos \lambda_1 + 2e^{\beta}_{zz} \cos o_3 \cos \lambda_3 \\ &+ e^{\beta}_{zx} (\cos \phi_3 \cos \lambda_1 + \cos \phi_1 \cos \lambda_3) \end{aligned}\right\} \quad (3)$$

where o_1 and o_3 are the angles between the slip plane normal and the x and z axes, respectively, and λ_1 and λ_3 are the angles between the slip direction and the x and z axis, respectively.

For the orientation of the slip plane and direction given earlier and to maintain continuity

$$e_t^{\alpha} = e_{zx}^{\alpha} = e_t^{\beta} = e_{zx}^{\beta} \quad (4)$$

Since these shear strains can be produced by a single shear stress σ_{zx}, we may write for each phase

$$e^{\alpha}_{xx} = s^{\alpha}_{55} \sigma^{\alpha}_{zx} \quad [a], \quad e^{\beta}_{zx} = s^{\beta}_{55} \sigma^{\beta}_{zx} \quad (b) \quad [5]$$

continuity is obtained when eq [5a] is set equal to eq [5b]. If $e^{\alpha}_{zx} \neq e^{\beta}_{zx}$, then interaction stresses will develop which will modify the magnitudes of σ^{α}_{zx} and σ^{β}_{zx} in order to produce equivalence of the shear strains. Further, if $e^{\beta}_{zx} > e^{\alpha}_{zx}$ then β will tend to increase e^{α}_{zx} and, therefore, effectively increases the shear stress on the α slip system.

PROCEDURE

A. Interface Plane of Alpha and Beta

Martensite in Ti-Mn alloys has been shown to have either a $\{334\}_\beta$ or a $\{344\}_\beta$ habit plane (14). It is most likely that martensite and Widmanstätten α have the same β habit plane (15) and have the same onientation relationships with respect to the parent β. Only the $\{334\}_\beta$ habit plane, however, has been reported for Widmanstätten α (9, 16, 17), and consequently $\{334\}_\beta$ is taken to be the plane of β parallel to the interface. If the Burgers orientation relation is arranged so that

$$(0001)_\alpha \;//\; (110)_\beta$$

$$[2\bar{1}\,\bar{1}\,0]_\alpha \;//\; [1\bar{1}\,\bar{1}]_\beta$$

then the plane of α parallel to $(\bar{3}34)_\beta$ is $(\bar{1}3\,580)$ as is shown in Fig. 2. If, however, the $[1\,\bar{2}\,10]_\alpha$ direction is made parallel to the $[1\,\bar{1}\,1]_\beta$, which also lies in $(110)_\beta$, then the plane of α parallel to $(\bar{3}34)_\beta$ is $(\bar{5}140)$. The existence of the $\{\bar{5}140\}_\alpha$ parallel to $\{334\}_\beta$ was originally reported by Albert (18) and in recent investigations (9, 17). The pole of the $(\bar{5}140)$ plane is shown in Fig. 2 and it is 11° away from $(\bar{1}3580)$.

Most of the calculation reported here have been made for the $(\bar{1}3\,580)_\alpha$ interface plane. It will be shown that at the point when there is maximum interaction between alpha and beta the difference between the elastic strains on the slip systems when calculated for the two interface planes of alpha is about 5%.

B. Elastic Constants

The five elastic compliances for single crystals of α (19) are s_{11} = 0.997, s_{12} = - 0.472, s_{13} = - 0.193, s_{33} = 0.688, s_{44} = 2.14 in units of 10^{-12} $cm^2/dyne$. Fisher and Dever (20) have measured the elastic stiffnesses of

β-Ti - 10 wt. % cr crystals at 25°C as $c_{11} = 1.331$, $c_{12} = 0.951$ and $c_{44} = 0.427$. In units of 10^{12} dynes/cm^2. When converted to elastic compliances, the values are $s_{11} = 1.857$, $s_{12} = -0.774$ and $s_{44} = 2.342$ in units of 10^{-12} cm^2/dyne. These compliances refer to the principal crysrallographic axes, indicated by squares in Fig. 2, x_o^α, y_o^α, z_o^α and x_o^β, y_o^β and z_o^β.

In the calculations made a series of axes, at various positions with respect to the interface were assumed. It was necessary to convert the elastic compliances to each of these axes. The necessary transformation equations can be derived according to procedures outlined by Zener (21) or Nye (22).

If one assumes that only a normal stress is applied on a crystal in a given direction and if this direction is set to be x'(y' and z' is obtained so that x'y'z' will form a right handed coordinate system) then to define the state of strain in the crystal it is necessary only to calculate the six elastic constants namely s'_{11}, s'_{21}, s'_{31}, s'_{41} s'_{51} and s'_{61} to find the six strains as shown below:

$$\left.\begin{aligned} &e_{x'x'} = s'_{11}\,\sigma_{x'x'},\ e_{y'y'} = s'_{21}\,\sigma_{x'x'},\ e_{z'z'} = s'_{31}\,\sigma_{x'x'} \\ &e_{y'z'} = s'_{41}\,\sigma_{x'x},\ e_{z'x'} = s'_{51}\,\sigma_{x'x'} \text{ and } e_{x'y'} = s'_{61}\,\sigma_{x'x'} \end{aligned}\right\} \quad (6)$$

where $\sigma_{x'x'}$ is the applied stress and is considered constant. The six elastic constants were calculated for both phases for a total 54 different directions, Fig. 2.

C. Elastic Strains Resolved into Interface and Slip Systems

Once the six elastic compliances for each stress direction for α and β have been calculated, the strains could be obtained from eq. [6]. The next step was to transform these strains into a new set of axes xyz such that xz

is the interface plane as indicated in Figs. 1 and 2. Since the transformation laws for such a tranformation of strains is the same for both the α and β phases one can avoid transforming the strains of all the 54 stress directions into the new set of axis xyz by examining the strains to obtain representative results. The elastic strains of the α and β phases for each stress direction of the 54 stress directions were compared and the stress directions for the transformation of strains were chosen so that in some stress directions maximum and in other directions minimum interactions was likely to occur.

The chosen stress directions namely x'_1, x'_5 etc. are circled as shown in Fig. 2. The strains in x'_1 y'_1 z'_1, in x'_5, y'_5, z'_5 etc. sets of axes were then transformed into the new set of axis x, y, z, Figs. 1 and 2. As indicated earlier, eq. [1], the strains which need to be considered for compability are e_{xx}, e_{zz} and e_{zx}, and these elastic strains for both the α and β phases have in turn, been resolved into 12 α slip systems, 3 prisom 3 basal and 6 pyramidal. It was assumed that the α slip systems had parallel counter parts in the β phase, although these planes and directions would not necessarily act as slip systems in the β, and elastic strain of β were resolved onto these "slip" systems. The total resolved compatibility shear strains on any given slip system were obtained from eq. [3].

D. Maximum Interaction Stress

An attempt was made to determine approximately the interaction stress corresponding to the stress direction, x'_{24} for which the difference between e_t^{α} and e_t^{β} for the slip system of α and β was found to be maximum. For α this slip system is designate E, $(0001)[1\bar{2}10]$, Table I. The corresponding "slip" system of beta is not of specific interest. The shear strains e_t^{α} for

slip system E and the corresponding e_t^{β} were determined. The corresponding values of the elastic compliances $s^{\alpha, E}$ and $s^{\beta, E}$ were calculated as 2.141 and 3.415 in units of 10^{-12} cm^2/dyne, respectively. Eastic shear stress-shear strains curves for E slip systems are shown in Fig. 4. From these two curves it is possible to make a first order calculation of the interaction stresses, as well be discussed in the results, by assuming that a stress of a specific magnitude is applied along the x'_{24} direction.

E. Interface Phase

Although the volume fraction of interface phase is quite small and its thickness is usually less than 0.4 μm (17), some consideration has been given to its possible role on producing interaction stresses because of the possibility that it could have a high yield strength and therefore withstand high total elastic stresses. When the interface phase is alpha (rather than the transitional fcc phase (17)), it has been reported to be either in $\{10\bar{1}1\}$ (10) or $\{10\bar{1}2\}$ (8, 9) twin relationship with respect to the primary α. The $\{10\bar{1}1\}$ twins have a Burgers orientation relationship with β(23) and hence these specific $\{10\bar{1}1\}$ twins have been considered in this anaylsis. It was not possible to ascertain which specific $\{10\bar{1}2\}$ twins were present and accordingly all six possibilities were considered, Fig. 3. Interactions have been determined only for the stress direction x'_{24}. The relative positions of the x_o^{α}, y_o^{α} and z_o^{α} change with respect to the x'_{24}, y'_{24}, z'_{24} coordinate system. The x_o^{G}, y_o^{G}, z_o^{G} are the new positions of the x_o^{α}, y_o^{α}, z_o^{α} positions for the twin G$(0\,1\,\bar{1}\,1)$. Once the new positions of x_o^{α}, y_o^{α}, z_o^{α} have been determined then the procedure, outlined previously for the determination of interactions, was followed.

RESULTS

A. Total Resolved Compatibility Shear Strains

The elastic compliances, and hence the strains, have been calculated for the 54 stress directions. For the twelve directions of interest the strains have been transformed to the x, y, z axes related to the interface, Figs. 1 and 2, and then the $e_{xx'}$ e_{zz} and e_{zx} strains were further resolved on to the twelve slip systems, previously given, for both the α and β phases, according to eq. [3]. The results are given in Tables 1a and 1b. The Schmid factors are given in Table 2. The Schmid factors have positive and negative signs because positive directions have been assigned to the slip directions irrespective of the applied stress. The last column of Table 1, contains comments indicating whether the interaction strains aid or oppose the applied strains induced directly from the applied stress. The interaction strains aid or add to the applied strains when the difference between the strains in β and α, $\Delta e = e_\beta - e_\alpha$, has the same sign as the applied strain. The interaction strains oppose the applied strains when this difference has a sign opposite to the applied strain.

In Tables 1a, 1b, and 3 the x'^{*}_{24} direction is for the case where the interface planes are $(\bar{5}\,140)_\alpha$ and $(\bar{3}\,34)_\beta$. For this pair of interface planes the Burgers orientation is

$$(0001)_\alpha \;//\; (110)_\beta$$

$$[1\bar{2}\,10]_\alpha \;//\; [1\bar{1}\,1]_\beta$$

It is to be noted that the x'^{*}_{24} directions is similar to the x'_{24} direction, i.e. both directions lie in their respective interface planes and are both 50° away from $[0001]_\alpha$ and $[110]_\beta$.

B. Total Resolved Compatibility Shear Strains for the Interface Phase

Table 3 gives the total resolved, compatibility shear strains resolved onto the twelve slip systems of α, designated A, B etc. The calculations were carried out in the same manner as for Table 1, for the direction x'_{24}.

C. Estimate of Compatibility Shear Stresses

When a given stress is applied in a given direction in α and β, the strains when resolved into the interface will generally not be the same. Accordingly some adjustment must be made in the interface strains of α and β with the result that interaction stresses will arise, as pointed out earlier.

When the adjustments have been made, all the compatibility strains will be equivalent and when resolved onto the parallel slip systems of α and β the elastic strains on these slip systems must also be equal.

Let us assume that a constant stress, say 103.4 MPa (15 ksi or 103.4 $\times 10^7$ dynes/cm^2) is applied to each phase along the x'_{24} direction. This stress will produce the strains $e_t^{\alpha, E}$ and $e_t^{\beta, E}$, see Table 1. If one assumes that equivalent shear stresses $\sigma^{\alpha, E}$ and $\sigma^{\beta, E}$ have been applied to produce these strains, then the $e_t^{\alpha, E}$ and $e_t^{\beta, E}$ positions will be located as shown in Fig. 4. It is assumed that there are equal volume fractions of each phase. Sine the shear stresses in each phases are parallel and the cross sectional areas are equal a decrease in stress in one component must be matched by an increase in stress in the other. Thus we may write

$$\Delta\sigma^{\alpha, E} = \Delta\sigma^{\beta, E} \tag{7}$$

$$\Delta\sigma^{\alpha, E} = \left(e_{t, f}^{\alpha, E} - e_t^{\alpha, E} \right) \frac{1}{s^{\alpha, E}} \tag{8}$$

$$\Delta\sigma^{\beta, E} = \left(e_t^{\beta, E} - e_{t, f}^{\beta, E} \right) \frac{1}{s^{\beta, E}} \tag{9}$$

Where $\Delta\sigma^{\alpha, E}$ and $\Delta\sigma^{\beta, E}$ are the changes in equivalent shear stress along the E slip system for α and β, respectively, $e_{t,f}^{\alpha, E}$ and $e_{t,f}^{\beta, E}$ are the final, equal shear strains on the E slip systems after compatibility has been established.

From eq's [7], [8] and [9] it follows that

$$e_{t,f}^{\alpha, E} = e_{t,f}^{\beta, E} = \frac{e_t^{\alpha, E} \cdot s^{\beta, E} + e_t^{\beta, E} \cdot s^{\alpha, E}}{s^{\alpha, E} + s^{\beta, E}} \qquad (10)$$

The strains $e_{t,f}^{\alpha, E}$ and $e_{t,f}^{\beta, E}$ are shown on their respective curves in Fig. 4. The change in stress is 14 MPa (2.0ksi, 14×10^7 dynes/cm^2 which is 30% of the resolved shear stress. This increment of stress in α adds to the applied stress and thus increases the total stress on the basal slip system E.

DISCUSSION

A. Effect of Stress Direction on Elastic Interactions

The interaction stresses are only a fraction of the shear stresses produced by the applied stress. Consequently, these stresses will be significant in initiating slip only for those slip systems for which the Schmid factors are highest. The interactions are highest for the stress directions x'_{58}, x'^{*}_{24} and x'_{24}, Table 1a and 1b, Fig. 2. For example, for stress direction x'_{24} the total resolved compatibility elastic strain on the E slip system of α and β are

$$e_t^{\alpha, E} = 0.978\ \sigma_{x'_{24}}$$

$$e_t^{\beta, E} = 1.718\ \sigma_{x'24}$$

$$\Delta e = e_t^{\beta, E} - e_t^{\alpha, E} = 0.740\ \sigma_{x'24}$$

The large value of Δe indicates that the elastic strins in β will strongly assist slip in α, since the signs of Δe and the Schmid factor are the same. The largest value of Δe is $\Delta e = 0.907\ \sigma_{x'58}$ for the E slip system and here β will also assist slip in α.

Interactions can also be quite high for x'_{52} and x'_{43}, but for these slip systems the Schmid factors are low.

The increases to the resolved shear stress of α by the elastic interaction was estimated to be 30% for x'_{24}, Fig. 4 on the E slip system, where the maximum interactions are found. Examination of Tables 1a and 1b indicates that the interactions on the E slip system are somewhat higher for the x'^{*}_{24} stress direction, which lies on the $(\bar{5}\ 140)_\alpha$ interface plane parallel to $(\bar{3}34)_\beta$. A calculations analogous to that for x'_{24} was also carried out for the x'_{58} directions, and the increment to the resolved shear stress of α was 35% , the maximum increment. The x'_{24}, x'^{*}_{24} and x'_{58} axes all lie near the $(\bar{1}3580)_\alpha$ interface plane, and lie between 40 and 50° to the pole of the basal plane. The x'_{43} and x'_{52} axis also lie within 40-50° of the basal plane pole, but along a different plane, Fig. 2.

Within a range of 10° to the basal plane pole, stress axes, x'_{28}, x'_{29}, x'_{59}, Fig. 2, the interactions are small, Tables 1a and 1b. When the stress axis lie in the basal plan, x'_{1}, x'_{5}, x'_{16}, x'_{20}, Fig. 2, there is no interaction for the basal slip system. For these stress axes some of the Schmid factors for the prism and pyramidal slip are high. In these cases the interaction stresses weakly oppose the applied stress. When compared to other slip systems interactions are strongest for the basal slip systems and thus slip on the basal slip systems can be most strongly aided by these stresses. Elastic interactions, although weak, can also assist pyramidal slip, see slip system U for stress axis x'_{24}, Table 1b. However, for

prism slip, elastic interactions only weakly oppose the strains resulting from applied stress, see slip system C for stress axis x'_1, Table 1a.

B. Slip in Colonies of Widmanstätten α and β

1. Role of Interaction Stresses

In the following discussion it is assumed, for lack of data, that the elastic constants of pure α (19) and β containing 10 wt % cr (20) apply for α and β phases of Ti-8 Al- 1Mo -IV, results from which alloy (24) are to be discussed here. The elastic interactions, which have been presented earlier, take place at a single α-β interface. In a colony of Widmanstätten α and β, the orientations of both α and β are constant. Thus, when significant interaction stresses are present, they occur at each interface and, thus, a long range elastic interaction stress is created.

Wojcik and Koss (24) have determined the resolved shear stress on the observed slip plane at the 0.2% yield stress for colonies of Widmanstätten α and β in a Ti-8 Al-1Mo-IV alloy. The orientations of the stress axis in a standard stereographic triangle are presented in Fig. 5 and the results are given in Table 4. It can be seen that there is a range of resolved shear stresses from 228 MPa for stress axis 15 to 463 MPa for stress axis 17.

To assess the role of the interface interactions in affecting these stresses the orientation of the stress axis with respect to the α-β interface must be considered. For stress axis 15 the pole of the β interface plane is 95° from the stress axis and for stress axis 17 the β interface pole is 77° away (24). From this information, and that of Fig. 5, axis 15 is located at x'_{58} and axis 17 is located at x'_{59} in Fig. 2.

Since the applied stresses are known for these stress axes, Table 4, calculations similar to those made for x'_{24} were carried out to ascertain the approximate interaction stresses. For stress axis x'_{58} the elastic

strain in β is higher than the strain in α, and if the volume fractions of α and β were equal, 90 MPa would be added to the nominal stress for slip in Table 4* for slip system E with the highest Schmid factor. For stress axis x'_{59}, β opposes α deformation and again for equal volume fractions of α and β, the decrease in nominal stress would be 29 MPa for slip system F, for which the Schmid factor is highest. It should be noted that when the interaction stress aids slip the stress required from the applied stress is reduced, and when the interaction stress opposes slip a greater applied stress is required.

It is clear that when the elastic interactions for stress axis x'_{58} and x'_{59} are considered the differences between resolved shear stresses for slip for axis 15 and 17 would be reduced. If the maximum interactions took place, then the stresses for slip would be

axis 15 (x'_{58}) : 363 MPa

axis 17 (x'_{59}) : 485 MPa

The difference in resolved shear stress, when elastic stresses are considered, would be about 34% compared to axis 15 stress and are 88.4% when the elastic stresses are not considered. One may reasonably question whether the maximum interaction is possible since the volume per cent of β is considerably less than 50, nevertheless, the trend must exist.

It also appears, reasonable to believe that, when the 0.2% yield stress is reached, slip in β as well as α is taking place. If slip in α is initiated

*Given the orientations shown in Fig. 5, calculations as to the resolved shear stress for axis 15 (x'_{58}) and 17 (x'_{59}) are somewhat different from those given in Table 4. They are respectively 273 and 514 MPa instead of 228 and 463 MPa.

before slip in β, then this slip in α, which will pile up dislocations at the interface, will help to initiate slip in β. This assistance would contribute to the lower resolved shear stress for axis 15. The stress axis x'_{58} (axis 15) and x'_{59} (axis 17) have been referred to the $(\bar{1}3580)_\alpha$ interface plane. There is little difference in the results, if they are oriented with respect to the $(\bar{5}140)_\alpha$ interface plane. It is of interest to note that the lowest observed resolved shear stress, axis 15, occurs when the assistance to slip in α by β is highest.

Table 4, shows that other slip systems may act in additions to basal slip. For appropriate oreintation, the Schmid factor, and elastic interactions may favor slip in these systems. It has been pointed out that the α-β interfaces are not always planar (24) and that this may contribute to the differences in stress noted in Table 4. Further, other factors now being considered (24), may reduce still more the differences in stress which remains unaccounted for by elastic interactions.

2. Role of the Interface Phase

For the stress direction x'_{24} calculations were carried out for 8 different kinds of twin interface orientations, Fig. 3. The calculated elastic strains are given in Table 3. To evaluate the effect of the total resolved compatibility strains of the twin, e_t^t, one must compare these strains with the corresponding strains in α for the x'_{24} axis, Tables 1a and 1b for all 12 slip systems of α and the corresponding 12 parallel slip systems of the twin. The comparsion will be made, for the moment, independent of the relative sizes of the two regions.

From Tables 1a, 1b and 3, it can be seen that the differences between e_t^α and e_t^t, in most instances, are very small. For example, compare the $e_t^{\alpha, E}$ for x'_{24}, Table 1a, with $e_t^{t, E}$ for the J twinning plane, Table 3:

$e_t^{\alpha, E} = 0.978\ \sigma\ x'_{24}$ and $e_t^{t, E} = 0.953\ \sigma\ x'_{24}$, a difference of $0.025\ \sigma\ x'_{24}$.

When there are significant differences, then the strains of the twins are in between the strains of the α and β phases. For $e_t^{\alpha, E}$, $e_t^{\beta, E}$ and $e_t^{t, E}$ for the N twinning plane of Table 3, the values are as follows.

$$e_t^{\alpha, E} = 0.978\ \sigma\ x'_{24}$$

$$e_t^{t, E} = 1.299\ \sigma\ x'_{24}$$

$$e_t^{\beta, E} = 1.718\ \sigma\ x'_{24}$$

In these circumstances the twin acts in the same direction as β, assisting deformation in α.

Only for the G twin does the twin oppose deformation of α and here the magnitude of the opposition is small. Compare the following e_t values.

$$\left.\begin{aligned} e_t^{\alpha, E} &= 0.978\ \sigma\ x'_{24} \\ e_t^{t, E} &= 0.831\ \sigma\ x'_{24} \end{aligned}\right\} \Delta e = -0.147\ \sigma\ x'_{24}$$

$$e_t^{\beta, E} = 1.718\ \sigma\ x'_{24}$$

However, the twin strongly opposes the strain in β and the net effect is that the assistance to slip in α by β is reduced. Thus interactions similar to those found at α/β interfaces can be found at twin/β and at α/twin interfaces.

The thickness of the twins can extend up to about $0.4\ \mu$m(17) which is much smaller than the thickness of α and β. Thus the role of twins in assisting or resisting deformation of α by β is likely to be quite limited.

Crystallographically the twins at the interface can readily permit transfer of slip from α to twins to β, because of the existence of the following relationships, Fig. 3.

$$(0001)_\alpha \;/\!/ \left\{ \begin{array}{l} \{10\bar{1}1\}_{\text{twin G, H}} \\ \text{or} \\ \{10\bar{1}0\}_{\text{twin I, J, K, L, M, N(within } 5^\circ)} \end{array} \right\} /\!/ \{110\}_\beta$$

$$\langle 11\bar{2}0\rangle_\alpha \;/\!/\; \langle 11\bar{2}0\rangle_{\text{twin G, H, I, J,}} \;/\!/ \langle 111\rangle_\beta$$

for twin planes M and N transfer of slip to β should be some what more difficult, because the $\langle 11\bar{2}0\rangle$ direction of both α and twin are about 11° from $\langle 111\rangle_\beta$. For the K and L twin planes transfer of slip from the twin to β can not easily be achieved because of the large angle between the slip directions, Fig. 3.

For the E slip system, $(0001)[1\bar{2}10]$, for which the elastic interactions are greatest, Fig. 3 indicates that $[1\bar{2}10]$ is about 11° away from $[1\bar{1}1]_\beta$ for M and N $\{10\bar{1}2\}$ twins, and thus, transfer of slip would be intermediate in difficulty. However, if, in setting up the Burgers orientation relationship, these two directions had been made parallel, the α habit plane would have become $(\bar{5}\,140)$ and the magnitude of the elastic interactions would have been about the same as for the $(\bar{1}\,\bar{3}\,580)_\alpha$ interface, as previous calculations have shown. In this case, slip tranfer would have been quite readily achieved for both $\{10\bar{1}1\}$ and $\{10\bar{1}2\}$ twins. Thus, depending on which twinning

system occurs, it is quite possible for the crystallography to permit ready transfer of slip.

For those instances where transfer of slip would be easy, only the dislocations, and defect structure of the twin, developed during its formation would serve as an obstacle to slip transfer.

C. Elevated Temperature Effects of Interface Stresses

In the preceding discussion on interaction stresses it has been pointed out that, at room temperature, β can assist slip in α, as a result of interaction stresses. At elevated temperatures, it has been reported that Widmanstätten structures have higher creep resistance than equiated structures. It has long been recognized that the α phase has higher creep resistance than the β phase. A change in morphology does not change the composition of the phases. Consequently, one may look to the difference on creep behavior of the two morphologies in terms of the structure.

One simple way of looking at the situation is to consider that the existence of the Widmanstätten structure reduces the path lengths of slip on the β and, as a reslult, increases the creep resistance.

Another point of view is that elastic interaction stresses may contribute to creep resistance. Although , β may assists deformation of α, α at the same time would impede deformation of β. At elevated temperatures, when β has less resistance to creep, the resistance to deformation in β, provided by α, would increase creep resistance. Further, since the interaction stresses occur over an entire colony, the whole region would be expected to be strengthened by the interaction stresses. In addition to the inherent behavior of each phase and the effect of interaction stresses, one would also expect that volume fraction of phases in the Widmanstätten colony structures would also be significant.

SUMMARY

1. The six elastic strains, associated with stress along a single normal axis, have been calculated for 54 different stress axes. These strains were then resolved along the α-β interface for twelve representative directions. Only those strains associated with compatibility were resolved onto twelve slip systems of α and a corresponding set of parallel slip systems in β. The slip systems, assumed for β, were not necessarily actual slip systems. From a comparison of these resolved elastic strains it was possible to determine whether the elastic strain in β would add to the elastic strain in α and, thereby, assist in the initiation of slip in α.

2. Calculations were carried out for the Burgers orientation, in which

$$(0001)_\alpha \;//\; \{110\}_\beta$$

$$<11\bar{2}0>_\alpha \;//\; <111>_\beta$$

and for the assumption that the interface plane of α parallel to $\{334\}_\beta$ was $\{\bar{1}3\,580\}_\alpha$. The alternate interface plane of α, $\{\bar{5}\,140\}_\alpha$, reported in the literature occurs when the second of the $<111>_\beta$ directions in $\{110\}_\beta$ is chosen. Calculations shows that, if $\{\bar{5}\,140\}_\alpha$ is the interface plane, there is very little difference in the magnitude and type of interaction stress.

3. Maximum elastic interactions between α and β were found when the stress axes were in or close to the interface plane. An estimate of the magnitude of these stresses, based on compatibility strains alone, indicated that the elastic interaction stresses could be 30-35% of the resolved shear stress.

4. It was found that β provided maximum interaction assistance to strain in α along the basal slip system $(0001)\,[\,\bar{1}2\bar{1}0\,]$. Interaction assistance was found to be smaller for prism and pyramidal slip.

5. Calculations for elastic interactions in colonies of Widmanstätten α and β were carried out for the alloy, Ti-8Al-1M0-IV, for which experimental data were supplied by Wojcik and Koss (24). It was found that the highest interaction assistance from β occurred for the basal slip systems for which the experimental resolved shear stress was least.

6. It was proposed that the elastic stresses at α-β interfaces of Widmanstätten structures, stresses which oppose slip in β, contribute to the greater creep resistance of Widmanstätten over equiaxed α-β structures at elevated temperatures.

ACKNOWLEDGEMENTS

Our interest in the problem was piqued by the earlier work of C.C. Wojcik and Professor Donald Koss to whom we wish to express our appreciation. We wish also to thank Prof. Koss for supplying the information from research on the resolved shear stress determination of Ti-8-1-1 colony structures. Thanks are due to Mr. Hiroshi Yaguchi, Graduate student of the Polytechnic Insitute of New York, for usefull discussions. The authors wish to express their appreciation to Dr. Bruce McDonald of the office of Naval Research for his continuing interest and encouragement. This work was supported by the Office of Naval Research on contract N-00014-75-C-0793.

REFERENCES

1. C. H. Wells and C. P. Sullivan: Trans. ASM 62, 263 (1969).
2. M. A. Greenfield and H. Margolin: Met Trans. 3, 2649 (1972).
3. D. Eylon, J. A. Hall, C. M. Pierce and , D. L. Ruckle: Met Trans. 7A 1817 (1976).
4. D. Eylon and J. A. Hall: Met Trans. 8A 981 (1977).
5. D. Shechtman and D. Eylon: Met Trans. 9A 1018 (1978).
6. D. Eylon and P.J. Bania: Met Trans. 9A 1273 (1978).
7. J. B. Newkirk and A. H. Geisler: Acta. Met. 1953, vol. 1, P. 370.
8. C. G. Rhodes and J. C. Williams: Met. Trans. A, 1975 vol. 6A, P. 1670.
9. C. G. Rhodes and J. C. Williams: Met. Trans. A, 1975, vol. 6A, P. 2103.
10. H. Margolin, E. Levine and, M. Young: Met. Trans. A, 1977, vol. 8A, P. 373.
11. R. E. Hook and J. P. Hirth: Acta. Met. Vol. 15, 1967, P. 535.
12. Y. Chuang and H. Margolin: Met Trans. vol. 4, 1973, P. 1905.
13. T. D. Lee and H. Margolin: Met. Trans. vol. 8A, 1977, P. 157.
14. Y. C. Liu and H. Margolin: Trans. AIME, 197, P. 667 (1953).
15. D. J. Maykuth, F. C. Holden, D. N. Williams, H. R. Ogden and, R. I. Jaffee: DMIC Report 136 B, Battle Memorial Institute, Columbus, Ohio, May, 1961.
16. G. Hahn, "The Habit Plane of Isothermal Alpha in Beta of Ti-Fe Alloys", Senior Thesis, New York University (June 1952).
17. C. G. Rhodes and N. E. Paton: Final Report Submitted to office of Naval Research, 1979; Contract No. N00014-76-C-0598.
18. P.A. Albert: Trans. TMS-AIME, 1953, vol. 197, P. 1449.
19. J. W. Flowers Jr., K.C.O. Brien and P. C. McEleney: J. Less-Common Metals, 7, P. 395 (1964).
20. E. S. Fisher and D. Dever: The Science Technology and Applications of Titanium Edited by R. I. Jaffee and N. E. Promisel, Pergamon Press, 1968, P. 373.

21. C. Zener: Elasticity and Anelasticity of Metals, the University of Chicago Press, Chicago 1948.

22. J. F. Nye: Physical Properties of Crystals, Oxford, Clarendon Press, 1957.

23. M. Young, E. Levine and, H. Margolin: Met. Trans. 1974, vol. 5, P. 1891.

24. C. C. Wojcik and D. A. Koss: Private Communication, Material to be Published.

FIGURES

Fig. 1. Geometry of the Alpha-Beta interface and coordinate axes.

Fig. 2. A stereographic projection showing the interface plane, $(\bar{1}3580)_\alpha$, $(\bar{3}34)_\beta$, Burgers orientation relationships, principal reference axes for elastic constants, x^α_o, y^α_o, z^α_o and x^β_o, y^β_o, z^β_o, and stress directions, x'.

Fig. 3. A stereographic projection showing the poles and planes of the $\{10\bar{1}1\}$ twins, G, H and the $\{10\bar{1}2\}$ twins, I, J, K, L, M, and N; and the crystallographic relationships between α and the twinned α.

Fig. 4. The determination of the magnitude of the interaction stress for the stress direction x'_{24} on the slip system E.

Fig. 5(24). The orientation of the stress axes in a standard HCP stereographic triangle for α in Widmanstatten colonies.

Table Ia and Ib: Total Resolved Compatibility Shear Strains of the α and β Phases (units of applied stress: 10^{12} dynes/sq. cm)

Table Ia: Basal and Prism Slip Systems

Stress Axis	I	$\left\|\frac{2\bar{1}\bar{1}0}{(01\bar{1}0)}\right\|_A$		$\left\|\frac{\bar{1}2\bar{1}0}{(\bar{1}010)}\right\|_B$		$\left\|\frac{\bar{1}\bar{1}20}{(1\bar{1}00)}\right\|_C$		$\left\|\frac{\bar{1}\bar{1}20}{(0001)}\right\|_D$		$\left\|\frac{1\bar{2}10}{(0001)}\right\|_E$		$\left\|\frac{\bar{1}\bar{1}20}{(0001)}\right\|_F$		Effect of β on the initiation of slip on α. For each slip system of α:
		$q_I^{\alpha,A}$	$q_I^{\beta,A}$	$q_I^{\alpha,B}$	$q_I^{\beta,B}$	$q_I^{\alpha,C}$	$q_I^{\beta,C}$	$q_I^{\alpha,D}$	$q_I^{\beta,D}$	$q_I^{\alpha,E}$	$q_I^{\beta,E}$	$q_I^{\alpha,F}$	$q_I^{\beta,F}$	
x'_1		$0.138\sigma x'_1$	$0.064\sigma x'_1$	$0.328\sigma x'_1$	$0.164\sigma x'_1$	$-0.456\sigma x'_1$	$-0.228\sigma x'_1$	0	0	0	0	0	0	A: Opposes V. weakly B, C: Opposes weakly D, E, F: No interaction
x'_5		$0.038\sigma x'_5$	$-0.124\sigma x'_5$	$-0.094\sigma x'_5$	$-0.314\sigma x'_5$	$0.138\sigma x'_5$	$0.440\sigma x'_5$	0	0	0	0	0	0	$\overline{\text{V}}$: Opposes V. weakly B: Aids weakly; C: Opposes significantly, D, E, F: No interaction
x'_{16}		$0.030\sigma x'_{16}$	$0.030\sigma x'_{16}$	$0.074\sigma x'_{16}$	$0.074\sigma x'_{16}$	$-0.302\sigma x'_{16}$	$-0.302\sigma x'_{16}$	0	0	0	0	0	0	No interactions
x'_{20}		$-0.276\sigma x'_{16}$	$-0.268\sigma x'_{16}$	$-0.674\sigma x'_{16}$	$-0.678\sigma x'_{16}$	$0.968\sigma x'_{16}$	$0.946\sigma x'_{16}$	0	0	0	0	0	0	A, B, C: Opposes V. weakly D, E, F: No interaction
x'_{24}		$-0.148\sigma x'_{24}$	$0.106\sigma x'_{24}$	$-0.352\sigma x'_{24}$	$0.268\sigma x'_{24}$	$0.498\sigma x'_{24}$	$0.374\sigma x'_{24}$	$0.140\sigma x'_{24}$	$0.258\sigma x'_{24}$	$0.978\sigma x'_{24}$	$1.718\sigma x'_{24}$	$0.838\sigma x'_{24}$	$1.460\sigma x'_{24}$	A, B: Opposes V. weakly C: Opposes weakly D: Aids weakly; E: Aids very strongly F: Aids Strongly
x'_{28}		$0.044\sigma x'_{28}$	$0.106\sigma x'_{28}$	$0.110\sigma x'_{28}$	$0.266\sigma x'_{28}$	$-0.152\sigma x'_{28}$	$-0.370\sigma x'_{28}$	$0.058\sigma x'_{28}$	$0.087\sigma x'_{28}$	$0.340\sigma x'_{28}$	$0.518\sigma x'_{28}$	$0.289\sigma x'_{28}$	$0.438\sigma x'_{28}$	A: Oppose V. weakly; B, C: Opposes weakly D: Aids V. weakly; E, F: Aids weakly
x'_{29}		$0.054\sigma x'_{29}$	$0.116\sigma x'_{29}$	$0.134\sigma x'_{29}$	$0.294\sigma x'_{29}$	$-0.188\sigma x'_{29}$	$-0.412\sigma x'_{29}$	0	0	0	0	0	0	Schmid factor from the applied stress is zero
x'_{36}		$-0.236\sigma x'_{36}$	$-0.220\sigma x'_{36}$	$-0.596\sigma x'_{36}$	$-0.556\sigma x'_{36}$	$0.832\sigma x'_{36}$	$0.778\sigma x'_{36}$	$-0.096\sigma x'_{36}$	$-0.168\sigma x'_{36}$	$-0.636\sigma x'_{36}$	$-1.128\sigma x'_{36}$	$-0.542\sigma x'_{36}$	$-0.952\sigma x'_{36}$	A, B, C: Opposes V. weakly; D: Aids V. weakly; E, F: Aids significantly
x'_{43}		$0.086\sigma x'_{43}$	$0.094\sigma x'_{43}$	$0.216\sigma x'_{43}$	$0.238\sigma x'_{43}$	$-0.308\sigma x'_{43}$	$-0.332\sigma x'_{43}$	0	$-0.100\sigma x'_{43}$	$0.001\sigma x'_{43}$	$-0.664\sigma x'_{43}$	$0.008\sigma x'_{43}$	$-0.568\sigma x'_{43}$	A, B, C: Aids V. weakly; D: Aids V. weakly; E: Aids strongly; F: Opposes strongly
x'_{52}		$0.098\sigma x'_{52}$	$0.086\sigma x'_{52}$	$0.250\sigma x'_{52}$	$0.216\sigma x'_{52}$	$-0.348\sigma x'_{52}$	$-0.302\sigma x'_{52}$	0	$0.100\sigma x'_{52}$	$-0.008\sigma x'_{52}$	$0.668\sigma x'_{52}$	0	$0.568\sigma x'_{52}$	A, B, C: Opposes V. weakly; D: Aids V. weakly; E: Aids strongly; F: Opposes strongly
x'_{58}		$-0.108\sigma x'_{58}$	$-0.058\sigma x'_{58}$	$-0.272\sigma x'_{58}$	$-0.144\sigma x'_{58}$	$0.380\sigma x'_{58}$	$0.202\sigma x'_{58}$	$0.148\sigma x'_{58}$	$0.272\sigma x'_{58}$	$0.948\sigma x'_{58}$	$1.848\sigma x'_{58}$	$0.800\sigma x'_{58}$	$1.570\sigma x'_{58}$	A: Opposes V. weakly; B, C: Opposes weakly D: Aids weakly; E, F: Aids very strongly
x'_{59}		$0.042\sigma x'_{59}$	$0.096\sigma x'_{59}$	$0.104\sigma x'_{59}$	$0.242\sigma x'_{59}$	$-0.144\sigma x'_{59}$	$-0.338\sigma x'_{59}$	$0.048\sigma x'_{59}$	$0.038\sigma x'_{59}$	$0.318\sigma x'_{59}$	$0.234\sigma x'_{59}$	$0.268\sigma x'_{59}$	$0.198\sigma x'_{59}$	A: Aids V. weakly; B: Opposes weakly C: Aids weakly, D: Aids V. weakly; E, F: Opposes V. weakly
x'_{24}		$-0.308\sigma x'_{24}$	$-0.248\sigma x'_{24}$	$-0.690\sigma x'_{24}$	$-0.144\sigma x'_{24}$	$0.50\sigma x'_{24}$	$0.380\sigma x'_{24}$	$0.352\sigma x'_{24}$	$0.618\sigma x'_{24}$	$1.038\sigma x'_{24}$	$1.822\sigma x'_{24}$	$0.686\sigma x'_{24}$	$1.203\sigma x'_{24}$	A, B: Opposes V. weakly; C: Opposes weakly, D: Aids weakly, E: Aids V. strongly F: Aids strongly.

Table 1b: Pyramidal Slip Systems

Stress Axis	$\lvert 2\bar{1}\bar{1}0\rvert_\alpha \,//\, \lvert 0\bar{1}11\rvert_\beta$ P		$\lvert 2\bar{1}\bar{1}0\rvert_\alpha \,//\, \lvert 01\bar{1}1\rvert_\beta$ Q		$\lvert 1\bar{2}10\rvert_\alpha \,//\, \lvert \bar{1}011\rvert_\beta$ R		$\lvert 1\bar{2}10\rvert_\alpha \,//\, \lvert 10\bar{1}1\rvert_\beta$ S		$\lvert \bar{1}\bar{1}20\rvert_\alpha \,//\, \lvert \bar{1}101\rvert_\beta$ W		$\lvert \bar{1}\bar{1}20\rvert_\alpha \,//\, \lvert \bar{1}\bar{1}01\rvert_\beta$ U		Effect of β on the initiation of slip in α for each slip system of α
	$c_i^{\alpha,P}$	$c_i^{\beta,P}$	$c_i^{\alpha,Q}$	$c_i^{\beta,Q}$	$c_i^{\alpha,R}$	$c_i^{\beta,R}$	$c_i^{\alpha,S}$	$c_i^{\beta,S}$	$c_i^{\alpha,W}$	$c_i^{\beta,W}$	$c_i^{\alpha,U}$	$c_i^{\beta,U}$	
x'_1	$-0.114\,x'_1$	$-0.056\,x'_1$	$0.114\,x'_1$	$0.056\,x'_1$	$-0.286\,x'_1$	$-0.143\,x'_1$	$0.216\,x'_1$	$0.142\,x'_1$	$-0.406\,x'_1$	$0.202\,x'_1$	$-0.406\,x'_1$	$-0.202\,x'_1$	P, Q: Opposes V. weakly; R, S: Opposes weakly; W, U: Opposes weakly
x'_5	$0.032\,x'_5$	$0.108\,x'_5$	$-0.032\,x'_5$	$-0.108\,x'_5$	$0.082\,x'_5$	$0.274\,x'_5$	$-0.082\,x'_5$	$-0.274\,x'_5$	$-0.116\,x'_5$	$-0.388\,x'_5$	$0.116\,x'_5$	$0.388\,x'_5$	P, Q: Opposes V. weakly R, S: Aids weakly, W, U: Opposes weakly
x'_{16}	$-0.026\,x'_{16}$	$-0.026\,x'_{16}$	$0.026\,x'_{16}$	$0.026\,x'_{16}$	$-0.064\,x'_{16}$	$-0.064\,x'_{16}$	$0.064\,x'_{16}$	$0.064\,x'_{16}$	$0.090\,x'_{16}$	$0.090\,x'_{16}$	$-0.090\,x'_{16}$	$-0.090\,x'_{16}$	No Interaction
x'_{20}	$0.240\,x'_{20}$	$0.236\,x'_{20}$	$-0.240\,x'_{20}$	$-0.236\,x'_{20}$	$0.602\,x'_{20}$	$0.590\,x'_{20}$	$-0.602\,x'_{20}$	$-0.590\,x'_{20}$	$-0.856\,x'_{20}$	$-0.838\,x'_{20}$	$0.856\,x'_{20}$	$0.838\,x'_{20}$	P, Q, R, S, W, U: Opposes V. weakly
x'_{24}	$0.143\,x'_{24}$	$0.218\,x'_{24}$	$-0.05\,x'_{24}$	$0.032\,x'_{24}$	$0.179\,x'_{24}$	$1.066\,x'_{24}$	$0.169\,x'_{24}$	$0.600\,x'_{24}$	$-0.038\,x'_{24}$	$0.377\,x'_{24}$	$0.837\,x'_{24}$	$1.034\,x'_{24}$	P: Aids V. weakly; Q: Opposes V. weakly R: Aids weakly, S: Aids significantly W: Opposes significantly; U: Aids weakly
x'_{28}	$-0.132\,x'_{28}$	$-0.050\,x'_{28}$	$0.063\,x'_{28}$	$0.134\,x'_{28}$	$0.0\,x'_{28}$	$0.050\,x'_{28}$	$0.260\,x'_{28}$	$0.511\,x'_{28}$	$0.275\,x'_{28}$	$0.566\,x'_{28}$	$0.005\,x'_{28}$	$-0.005\,x'_{28}$	P, Q: Aids V. weakly. R: Opposes V. weakly, S, W, Aids weakly, U: Opposes V. weakly
x'_{29}	$-0.023\,x'_{29}$	$-0.05\,x'_{29}$	$0.023\,x'_{29}$	$0.05\,x'_{29}$	$-0.058\,x'_{29}$	$-0.128\,x'_{29}$	$0.058\,x'_{29}$	$0.128\,x'_{29}$	$0.083\,x'_{29}$	$0.182\,x'_{29}$	$-0.083\,x'_{29}$	$-0.182\,x'_{29}$	Schmid factor from the applied stress is zero
x'_{36}	$0.166\,x'_{36}$	$0.112\,x'_{36}$	$-0.253\,x'_{36}$	$-0.275\,x'_{36}$	$0.203\,x'_{36}$	$-0.06\,x'_{36}$	$-0.828\,x'_{36}$	$-1.027\,x'_{36}$	$-1.0\,x'_{36}$	$-1.14\,x'_{36}$	$0.414\,x'_{36}$	$0.226\,x'_{36}$	P: Opposes V. weakly; Q: Aids V. weakly, R: Opposes weakly, S, W: Aids weakly; U: Opposes weakly
x'_{43}	$-0.075\,x'_{43}$	$-0.11\,x'_{43}$	$0.075\,x'_{43}$	$0.034\,x'_{43}$	$-0.187\,x'_{43}$	$-0.529\,x'_{43}$	$0.187\,x'_{43}$	$-0.115\,x'_{43}$	$0.266\,x'_{43}$	$-0.021\,x'_{43}$	$-0.266\,x'_{43}$	$-0.568\,x'_{43}$	P, Q: Aids V. weakly;R:Aids significantly; S: Opposes significantly, W: Opposes weakly; U: Aids significantly
x'_{52}	$-0.075\,x'_{52}$	$-0.026\,x'_{52}$	$0.075\,x'_{52}$	$0.124\,x'_{52}$	$-0.217\,x'_{52}$	$0.136\,x'_{52}$	$0.216\,x'_{52}$	$0.511\,x'_{52}$	$0.308\,x'_{52}$	$0.545\,x'_{52}$	$-0.308\,x'_{52}$	$0.808\,x'_{52}$	P, Q: Aids weakly; R: Opposes significantly, S: Aids weakly, W: Aids weakly U: Opposes weakly
x'_{58}	$0.163\,x'_{58}$	$0.185\,x'_{58}$	$-0.026\,x'_{58}$	$0.084\,x'_{58}$	$0.695\,x'_{58}$	$1.021\,x'_{58}$	$0.220\,x'_{58}$	$0.770\,x'_{58}$	$0.052\,x'_{58}$	$0.583\,x'_{58}$	$0.723\,x'_{58}$	$0.94\,x'_{58}$	P: Aids V. weakly, Q: Opposes weakly R: Aids significantly, S: Aids strongly W: Opposes strongly, U: Aids weakly
x'_{59}	$-0.013\,x'_{59}$	$-0.06\,x'_{59}$	$0.05\,x'_{59}$	$0.108\,x'_{59}$	$0.066\,x'_{59}$	$-0.097\,x'_{59}$	$0.245\,x'_{59}$	$0.323\,x'_{59}$	$0.26\,x'_{59}$	$0.395\,x'_{59}$	$0.083\,x'_{59}$	$-0.202\,x'_{59}$	P: Aids V. weakly, Q: Opposes V. weakly R: Opposes weakly, S: Aids V. weakly, W: Aids weakly, U: Opposes weakly
x'_{24}	$0.179\,x'_{24}$	$0.218\,x'_{24}$	$-0.05\,x'_{24}$	$0.032\,x'_{24}$	$0.179\,x'_{24}$	$1.066\,x'_{24}$	$0.169\,x'_{24}$	$0.600\,x'_{24}$	$-0.038\,x'_{24}$	$0.377\,x'_{24}$	$0.837\,x'_{24}$	$1.034\,x'_{24}$	P: Aids V. weakly, Q: Opposes V. weakly, R: Aids weakly, S: Aids significantly, W: Opposes significantly, U: Aids weakly

Calculations for $(\bar{3}140)_\alpha$ // to $(\bar{3}34)_\beta$ as the interface plane and $\lvert 1\bar{2}10\rvert_\alpha$ // to $\lvert \bar{1}\bar{1}1\rvert_\beta$

If $\lvert c_i^\alpha \cdot c_i^\beta\rvert$ is $\leq 0.1 \cdot x'$ very weak; $> 0.1 \cdot x'$ and $\leq 0.3 \cdot x'$ weak; $> 0.3 \cdot x'$ and $\leq 0.5 \cdot x'$ significant; $> 0.5 \cdot x'$ and $\leq 0.7 \cdot x'$ strong; $> 0.7 \cdot x'$ very strong

Table 2: Schmid Factors for the twelve Parallel Slip Systems of α and β.*

Slip System	Stress Directions												
	x'_1	x'_5	x'_{16}	x'_{20}	x'_{24}	x'_{28}	x'_{29}	x'_{36}	x'_{43}	x'_{52}	x'_{58}	x'_{59}	x'_{24} **
A	0.138	0.497	-0.347	-0.138	-0.079	-0.005	0	-0.121	0.0554	0.079	-0.207	0.043	-0.186
B	0.347	-0.294	0.485	-0.347	-0.207	-0.010	0	-0.306	0.146	0.201	-0.051	-0.017	-0.107
C	-0.485	-0.203	-0.138	0.485	0.283	0.015	0	0.423	-0.195	-0.283	0.254	-0.025	0.287
D	0	0	0	0	0.067	0.026	0	-0.045	-0.487	0.485	0.207	-0.207	0.166
E	0	0	0	0	0.455	0.163	0	-0.299	-0.185	0.183	0.493	0.058	0.492
F	0	0	0	0	0.387	0.137	0	-0.252	0.291	-0.302	0.283	0.272	0.321
P	-0.121	-0.439	0.302	0.121	0.102	0.017	0	0.084	-0.289	0.163	0.283	-0.138	0.244
Q	0.121	0.439	-0.302	-0.121	-0.037	0.009	0	-0.128	-0.186	0.307	-0.080	-0.063	-0.082
R	-0.303	0.258	-0.429	0.302	0.195	0.067	0	0.122	-0.216	-0.088	0.288	0.044	0.336
S	0.303	-0.258	0.429	-0.302	0.043	0.067	0	-0.411	0.038	0.265	0.197	0.013	0.146
W	0.420	0.170	0.121	-0.429	-0.063	0.053	0	-0.498	0.316	0.106	-0.092	0.173	-0.104
U	-0.420	-0.170	-0.121	0.429	0.433	0.079	0	0.252	-0.038	-0.394	0.362	0.106	0.410

* The "slip" systems of β are taken to be parallel to those of α and are considered slip systems whether or not they actually are.

** Calculations for $(\bar{5}140)_\alpha \;//\; (\bar{3}34)_\beta$ as the interface plane and $[1\bar{2}10]_\alpha \;//\; [\bar{1}11]_\beta$

Table 3: Total Resolved compatibility shear strains on twin "slip" systems*, parallel to those of α for the stress direction x'_{24}

Twins Planes of α	$e^{t,A}_t$	$e^{t,B}_t$	$e^{t,C}_t$	$e^{t,D}_t$	$e^{t,E}_t$	$e^{t,F}_t$	$e^{t,P}_t$	$e^{t,Q}_t$	$e^{t,R}_t$	$e^{t,S}_t$	$e^{t,W}_t$	$e^{t,U}_t$
$(0\,1\,\bar{1})$ G	$-0.084\sigma_{x'_{24}}$	$-0.210\sigma_{x'_{24}}$	$0.294\sigma_{x'_{24}}$	$0.125\sigma_{x'_{24}}$	$0.831\sigma_{x'_{24}}$	$0.706\sigma_{x'_{24}}$	$0.134\sigma_{x'_{24}}$	$-0.013\sigma_{x'_{24}}$	$0.586\sigma_{x'_{24}}$	$0.219\sigma_{x'_{24}}$	$0.082\sigma_{x'_{24}}$	$0.603\sigma_{x'_{24}}$
$(0\,\bar{1}\,1)$ H	$-0.124\sigma_{x'_{24}}$	$-0.314\sigma_{x'_{24}}$	$0.438\sigma_{x'_{24}}$	$0.163\sigma_{x'_{24}}$	$1.086\sigma_{x'_{24}}$	$0.923\sigma_{x'_{24}}$	$0.188\sigma_{x'_{24}}$	$-0.030\sigma_{x'_{24}}$	$0.799\sigma_{x'_{24}}$	$0.254\sigma_{x'_{24}}$	$0.060\sigma_{x'_{24}}$	$0.835\sigma_{x'_{24}}$
$(0\,1\,\bar{2})$ I	$-0.094\sigma_{x'_{24}}$	$-0.236\sigma_{x'_{24}}$	$0.330\sigma_{x'_{24}}$	$0.151\sigma_{x'_{24}}$	$1.003\sigma_{x'_{24}}$	$0.853\sigma_{x'_{24}}$	$0.155\sigma_{x'_{24}}$	$-0.009\sigma_{x'_{24}}$	$0.691\sigma_{x'_{24}}$	$0.281\sigma_{x'_{24}}$	$0.122\sigma_{x'_{24}}$	$0.705\sigma_{x'_{24}}$
$(0\,\bar{1}\,2)$ J	$-0.086\sigma_{x'_{24}}$	$-0.216\sigma_{x'_{24}}$	$0.302\sigma_{x'_{24}}$	$0.143\sigma_{x'_{24}}$	$0.953\sigma_{x'_{24}}$	$0.810\sigma_{x'_{24}}$	$0.144\sigma_{x'_{24}}$	$-0.006\sigma_{x'_{24}}$	$0.65\sigma_{x'_{24}}$	$0.275\sigma_{x'_{24}}$	$0.126\sigma_{x'_{24}}$	$0.66\sigma_{x'_{24}}$
$(\bar{1}\,1\,2)$ K	$-0.106\sigma_{x'_{24}}$	$-0.266\sigma_{x'_{24}}$	$0.372\sigma_{x'_{24}}$	$0.182\sigma_{x'_{24}}$	$1.214\sigma_{x'_{24}}$	$1.032\sigma_{x'_{24}}$	$0.181\sigma_{x'_{24}}$	$-0.004\sigma_{x'_{24}}$	$0.82\sigma_{x'_{24}}$	$0.357\sigma_{x'_{24}}$	$0.170\sigma_{x'_{24}}$	$0.830\sigma_{x'_{24}}$
$(1\,\bar{1}\,2)$ L	$-0.102\sigma_{x'_{24}}$	$-0.254\sigma_{x'_{24}}$	$0.356\sigma_{x'_{24}}$	$0.177\sigma_{x'_{24}}$	$1.181\sigma_{x'_{24}}$	$1.003\sigma_{x'_{24}}$	$0.174\sigma_{x'_{24}}$	$-0.003\sigma_{x'_{24}}$	$0.794\sigma_{x'_{24}}$	$0.350\sigma_{x'_{24}}$	$0.172\sigma_{x'_{24}}$	$0.801\sigma_{x'_{24}}$
$(\bar{1}\,0\,2)$ M	$0.106\sigma_{x'_{24}}$	$-0.266\sigma_{x'_{24}}$	$0.370\sigma_{x'_{24}}$	$0.192\sigma_{x'_{24}}$	$1.281\sigma_{x'_{24}}$	$1.088\sigma_{x'_{24}}$	$0.185\sigma_{x'_{24}}$	$-0.001\sigma_{x'_{24}}$	$0.851\sigma_{x'_{24}}$	$0.390\sigma_{x'_{24}}$	$0.200\sigma_{x'_{24}}$	$0.855\sigma_{x'_{24}}$
$(1\,0\,\bar{2})$ N	$-0.108\sigma_{x'_{24}}$	$-0.270\sigma_{x'_{24}}$	$0.378\sigma_{x'_{24}}$	$0.195\sigma_{x'_{24}}$	$1.299\sigma_{x'_{24}}$	$1.104\sigma_{x'_{24}}$	$0.188\sigma_{x'_{24}}$	$-0.001\sigma_{x'_{24}}$	$0.865\sigma_{x'_{24}}$	$0.395\sigma_{x'_{24}}$	$0.201\sigma_{x'_{24}}$	$0.870\sigma_{x'_{24}}$

* The "slip" systems of Twin are taken to be parallel to those of α and are considered slip systems whether or not they actually are.

TABLE 4 (24)

Compressive Yield Stress and Resolved Shear Stress on the Observed Slip Planes. Sample quenched from 760°C unless otherwise noted.

Sample Number	0.2% Yield Stress	Resolved Shear Stress on Observed Slip Plane
6	1160 MPa	414 MPa
7	634	312
8	2190	245
9*	612	281
10†	731	348
11	876	341
12*†	724	344
13†	1610	394
15	554	228
17	1890	463
19†	1480	454
20	605	285
21	590	262
22*	636	251

*These samples did not slip on the (0001) plane.

†Heat treated at 925°C and quenched.

FIGURE 1.

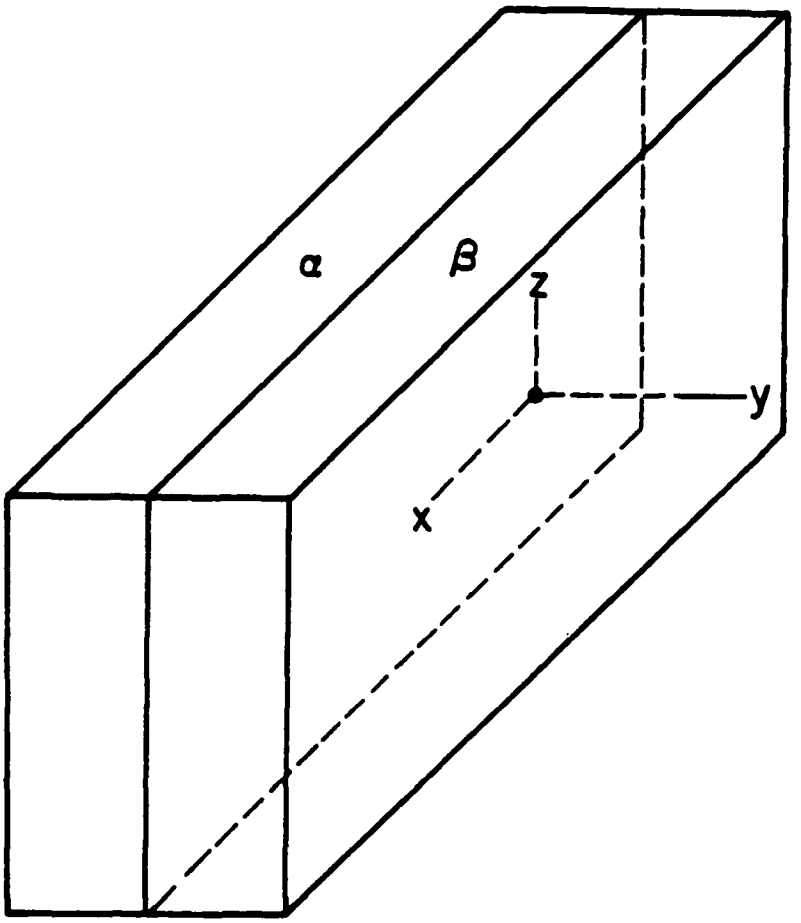

FIGURE 2

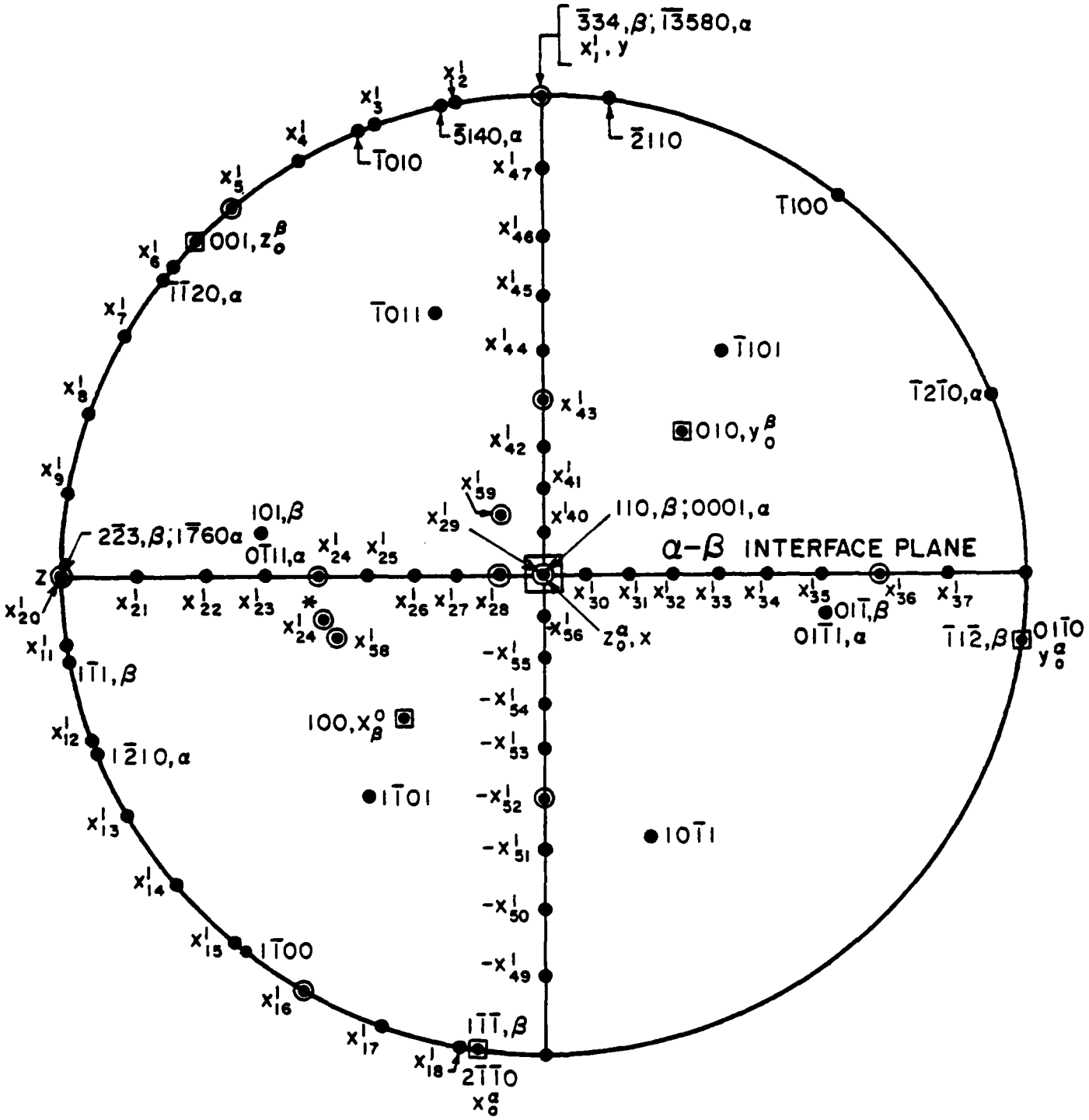
$\bar{3}34,\beta;\bar{1}3580,\alpha$
x_1^1, y
x_2^1
x_3^1
x_4^1
x_5^1
x_6^1
x_7^1
x_8^1
x_9^1
$\bar{5}140,\alpha$
$\bar{2}110$
$\bar{T}010$
$001, z_o^\beta$
$\bar{1}\bar{1}20,\alpha$
$T100$
x_{47}^1
x_{46}^1
x_{45}^1
x_{44}^1
x_{43}^1
x_{42}^1
x_{41}^1
$\bar{T}011$
$\bar{T}101$
$\bar{T}2\bar{1}0,\alpha$
$010, y_o^\beta$
x_{59}^1
x_{29}^1
x_{40}^1
$101,\beta$
$110,\beta;0001,\alpha$
$2\bar{2}3,\beta;\bar{1}760\alpha$
$0\bar{1}11,\alpha$
x_{24}^1
x_{25}^1
$\alpha-\beta$ INTERFACE PLANE
Z
x_{20}^1
x_{21}^1
x_{22}^1
x_{23}^1
x_{26}^1
x_{27}^1
x_{28}^1
x_{30}^1
x_{31}^1
x_{32}^1
x_{33}^1
x_{34}^1
x_{35}^1
x_{36}^1
x_{37}^1
$0\bar{1}\bar{1},\beta$
$0\bar{1}\bar{1},\alpha$
$\bar{1}\bar{1}2,\beta$
$01\bar{1}0$
y_o^α
x_{24}^1
x_{58}^1
x_{56}^1
z_o^α, x
x_{11}^1
$1\bar{1}1,\beta$
$-x_{55}^1$
$-x_{54}^1$
$100, x_\beta^0$
x_{12}^1
$1\bar{2}10,\alpha$
$-x_{53}^1$
$1\bar{1}01$
$-x_{52}^1$
x_{13}^1
$10\bar{1}1$
$-x_{51}^1$
x_{14}^1
$-x_{50}^1$
x_{15}^1
$1\bar{1}00$
$-x_{49}^1$
x_{16}^1
x_{17}^1
$1\bar{1}\bar{1},\beta$
x_{18}^1
$2\bar{1}\bar{1}0$
x_o^α

FIGURE 3

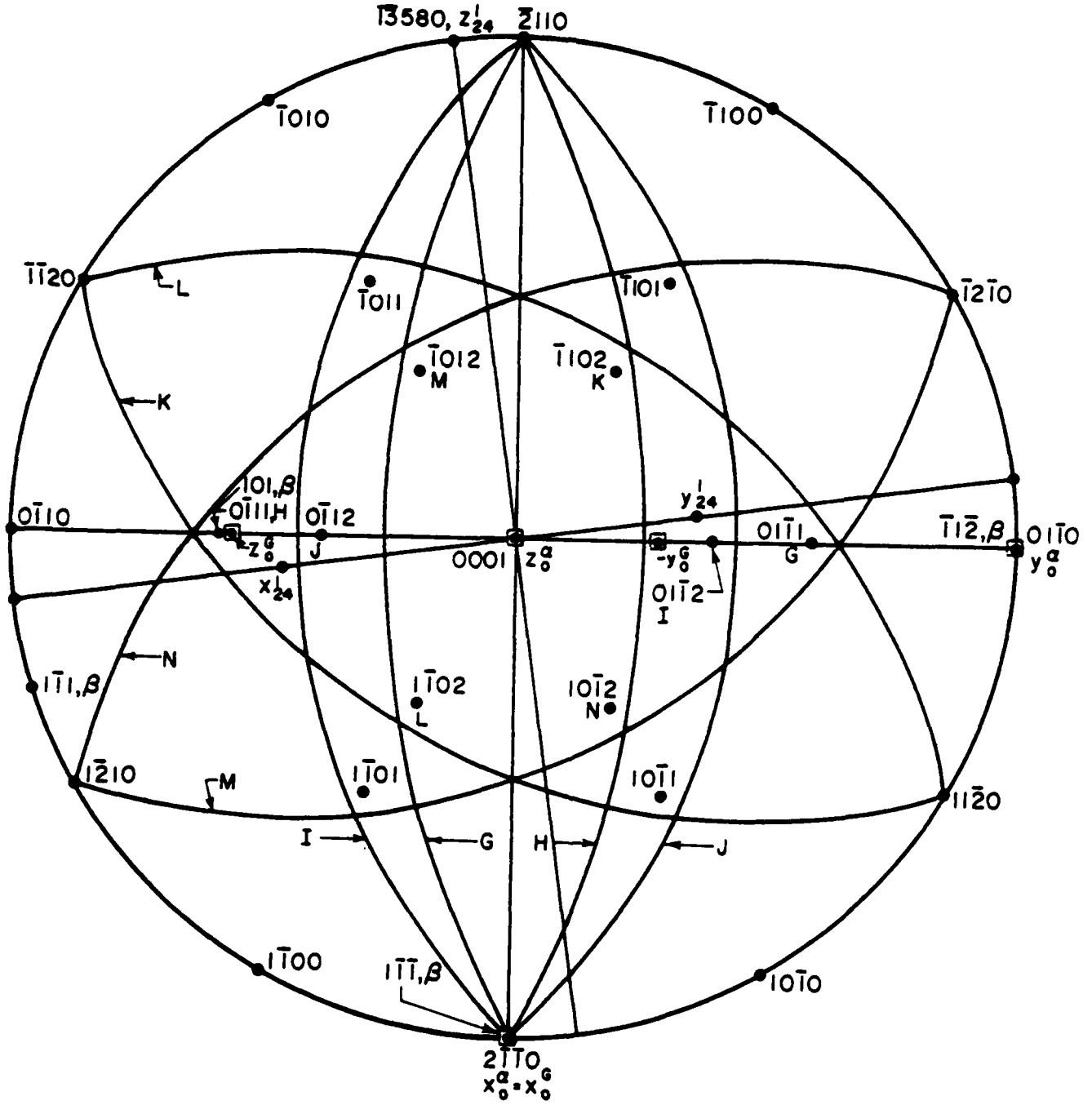
$\bar{1}3580, z^{I}_{24}$
$\bar{2}110$
$\bar{1}010$
$\bar{1}100$
$\bar{1}\bar{1}20$
L
$\bar{1}011$
$\bar{1}101$
$\bar{1}2\bar{1}0$
$\bar{1}012$
M
$\bar{1}102$
K
K
$101,\beta$
$0\bar{1}11,H$
$0\bar{1}10$
$0\bar{1}12$
z^{G}_{0}
J
x^{I}_{24}
0001
z^{α}_{0}
y^{I}_{24}
$-y^{G}_{0}$
$01\bar{1}1$
G
$\bar{1}\bar{1}2,\beta$
$01\bar{1}0$
y^{α}_{0}
$01\bar{1}2$
I
N
$1\bar{1}1,\beta$
$1\bar{1}02$
L
$10\bar{1}2$
N
$1\bar{2}10$
M
$1\bar{1}01$
$10\bar{1}1$
$11\bar{2}0$
I
G
H
J
$1\bar{1}00$
$1\bar{1}\bar{1},\beta$
$10\bar{1}0$
$2\bar{1}\bar{1}0$
$x^{\alpha}_{0} = x^{G}_{0}$

FIGURE 4

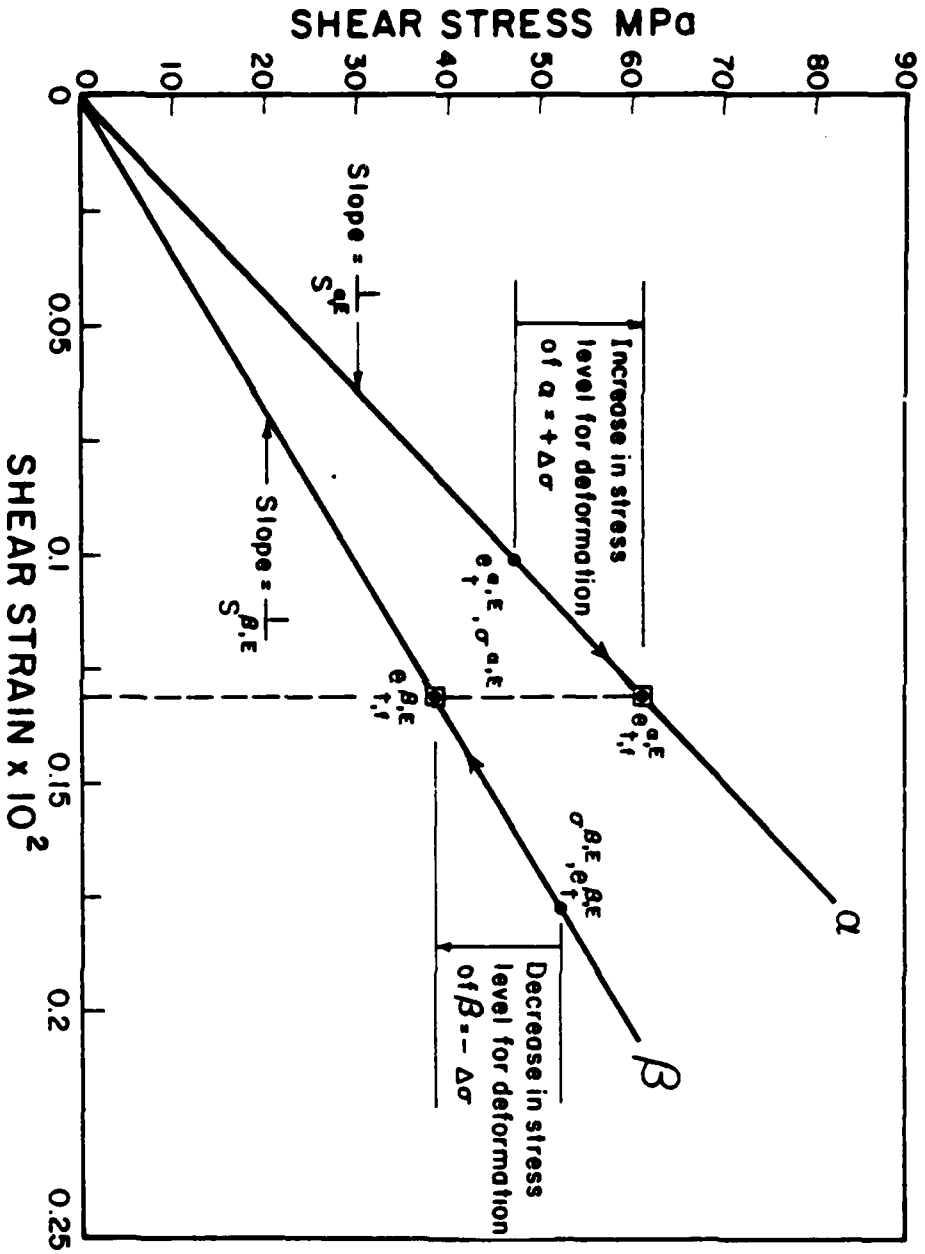
SHEAR STRESS MPa
0
10
20
30
40
50
60
70
80
90
SHEAR STRAIN x 10²
0
0.05
0.1
0.15
0.2
0.25
Slope = 1/S^αE
Slope = 1/S^βE
Increase in stress level for deformation of α = +Δσ
Decrease in stress level for deformation of β = -Δσ
α
β

FIGURE 5

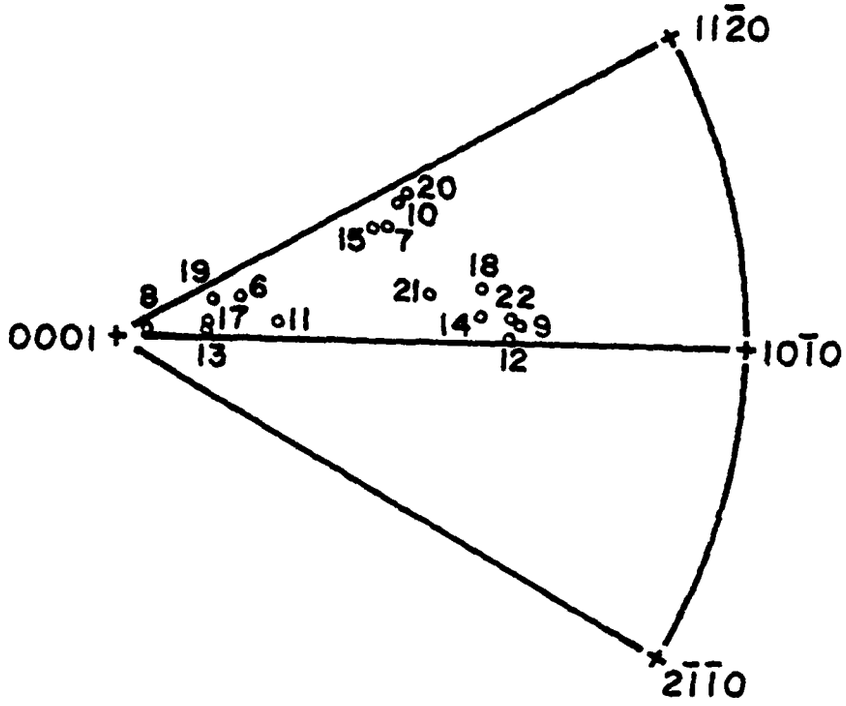
11$\bar{2}$0
20
10
7
19
8
6
18
21
22
17
11
14
9
13
12
0001
10$\bar{1}$0
2$\bar{1}\bar{1}$0

PART-II: FINITE ELEMENT METHOD (FEM) CALCULATIONS OF STRESS-STRAIN BEHAVIOR OF ALPHA-BETA Ti-Mn ALLOYS

ABSTRACT

By use of a NASTRAN (18) Computer Program, the Finite Element Method (FEM) has been employed to calculate the effect of particle size, matrix and volume fraction on the stress-strain relations of $\alpha-\beta$ titanium alloys. It was found that for a given volume fraction, the calculated stress-strain curve was higher for a finer particle size than for a coarse particle size within the range of the strains considered, and this behavior was seen for all the different volume fraction alloys considered. For a 50:50 vol % $\alpha-\beta$ alloy, the stress-strain curve with β, the stronger phase, as the matrix was higher than that with α, the softer phase, as the matrix. The calculated stress-strain curves for four different vol. % α alloys were compared with their corresponding experimental curves and in general good agreement was found. Whenever there were discrepancies, they were discussed by comparing the morphology of the mesh used in the calculations with the morphology of the actual materials.

Two ductile phase structures occur in many technologically important alloys. Increasing interest is developing in calculating the stress-strain behavior of the two-phase structures from the stress-strain curves of the component phases. In the present calculations FEM has been employed to calculate the effect of particle size, matrix and volume fraction of phases on the stress-strain behavior of α -β Ti alloys. In Part I, stress-strain relations will be shown and compared with the experimental curves for 4 different volume fractions. In Part II, stress-strain distributions will be shown and strain distributions will be compared with experimentally determined strain distributions.

Two simple hypotheses have been suggested by Dorn and Starr (1) to calculate the stress-strain curve of a two ductile phase mixture from the stress-strain curve of each phase and volume fractions: one is based on constant strain in each phase and the other is based on constant stress in each phase. Usually, the experimental curves of the two phase mixtures will lie somewhere between the two curves which are calculated according to the above two hypotheses, a fact that Dorn and Starr anticipated.

Davies (2,3,4) studied the deformation behavior of dual phase, ferrite-martensite, steels and have found that the 0.2% YS linearly varied with the volume fraction of the martensite, and followed a law of mixture rule. Interestingly, he (2,3,4) also found that the tensile strength and ductility of the dual phase steels are in agreement with the theory of Mileiko (5) and Garmong and Thompson (6). Since this theory (5,6) has been developed for mechanical properties of fiber composites of two ductile phases tested in tension parallel to the fiber

axis, it will have only a limited applicability because it (5,6) does not consider the morphology of the phases, which can effect the stress-strain behavior, as will be shown later.

Tomota et al. (7) have calculated the flow-stresses of alloys consisting of two ductile phases, α-γ Fe-Cr-Ni alloys on the basis of a continuum model where the internal stress produced by the inhomogeneous distribution of plastic strain is taken into account. They (7) have found that the calculated curve of the two-phase alloy was almost identical with that constructed by the simple equal strain model but the authors caution that there are circumstances where the material would not behave as if constant strain existed.

Fischmeister et al. (8), Karlsson and Sundstrom (9), and Fischmeister and Karlsson (10) have recently applied the FEM (11) to calculate the stress-strain curve of the soft matrix-hard particle, ferrite-martensite structures with 30 volume percent of martensite. In a previous investigation (12), FEM has been applied to calculate the stress-strain curve of a soft particle-hard matrix, α-β Ti-Mn alloy with 16.6 vol.% α, and it was shown that the calculated curve lay below the experimental stress-strain curve, Fig. 7. This difference was attributed to two factors. The first was the fact that the stress-strain curves of "single" phase α and β phases were used for the calculations (12). Since the grain sizes of both the "single phase" α and β was larger than the grain sizes of these phases in the duplex alloy (13), the calculated curve might have been lower than the experimental curve. The second factor was that the presence of the interface phase (14-16) might have contributed to the strength of the

duplex alloy (17) thereby raising the experimental curve above the calculated curve, which did not consider this structure. In the present calculations the first factor has been considered and the stress-strain curve has been recalculated. The second factor is not considered, since it is expected that the interface phase would make only a small contribution to the mechanical properties of α -β Ti-Mn alloys. Other factors, namely the effect of particle size and matrix which were not considered in the previous analysis (12), have been taken into account in the present analysis. In addition the calculations were made not only for the 16.3 vol.% α alloy but also for the 80, 63 and 41 vol. % α, and all the calculations have been compared with their corresponding experimental curves.

PROCEDURE

The procedure used in the present calculations is essentially similar to the one used in the previous calculations (12) and hence will be described only briefly here. However, there are some modifications and a check which will be described. NASTRAN (18) computer program, in particular rigid format No. 6 called "piecewise linear analysis", has been used for the solution of the elasto-plastic problem. An IBM 360/65 computer has been used. For all the calculations a uniform mesh of 392 triangular two dimensional (plane stress) plate elements, Fig. 1 was used, and the volume fraction, particle size and shape could be varied by designating each triangle either α or β, Figs. 1 to 6. The node J in Figs. 1 to 6 is considered fixed and all the other nodes along the line $\overline{AB}$ can move

only in the x direction. All the other nodes can move either in the x or y directions.

In the previous calculation (12) the nodes along the line $\overline{CD}$ moved independently in the x and y directions. Excessive differences in the y displacements in this edge $\overline{CD}$ were found (12) beyond the stress level 758 MPa (110 KSi), which is not expected in the real specimens. Thus all the calculations had to be restricted to 758 MPa (12). In the present analysis this problem was overcome through a multipoint constraint such that the nodes along the edge $\overline{CD}$ have the same y displacement at any stage of deformation whereas all the nodes other than the nodes in the lines $\overline{AB}$ and $\overline{CD}$ still can move freely either in x or y directions. This multipoint constraint was not incorporated in the calculations of the matrix effect, Fig. 4, where the previous procedure (12) was followed.

The input stress-strain curves for α and β phases that were used for all the calculations, except for the calculations of the matrix effect, Fig. 4 and 9, are shown in Fig. 7. The α stress-strain curve which corresponds to an α grain size, D, of 3μm* has been derived from the stress-strain curves of larger grain sizes, by extrapolating the flow stress vs. $D^{-1/2}$ plots for specific strains. It is to be noted that the flow stress dependency on grain size of α was found to be small and is close to that found by Jones and Conrad (19) for Iodide α titanium, even though the authors α titanium had an oxygen

---

*The α grain size of the alloys, the stress-strain curves of which are shown in Fig. 12, varied from 3 to 6 μm. This variation in the α grain size does not significantly effect the calculated curves which are also shown in Fig. 12.

content of 800 p.p.m. The flow stress dependency on grain size of β titanium was found to be negligibly small. However, in the present calculations the stress-strain curve of β, Fig. 7, without any α was used, unlike the previous calculations (12) where the β had about 4 vol. % α. In brief, the α and β curves used in the present calculations, Fig. 7, are slightly higher than the curves used in the previous calculations (12). For example, at a total strain of 0.015, the flow stress difference for α curves is 59 MPa (8.5 KSi) and the flow stress difference for β curves is 31 MPa (4.5 KSi); while the differences in the elastic part of the curves are negligibly small. As mentioned before, the α and β curves of the previous calculations (12) were used in the calculations of matrix effect, Figs. 4 and 9.

The load was applied uniformly at the nodes of the edge $\overline{CD}$ and was increased by predetermined increments where the first loading condition is such that all the stresses would be in the elastic region. For plotting the stress-strain curves, Figs. 7, 8, 10 and 12, the stresses are known for each loading condition, and the strains are calculated from the common displacement of the nodes of the line $\overline{CD}$ and the initial length AC, Figs. 1, 2, 3, 5 and 6. For calculating the stress-strain curve of the matrix effect (Fig. 9), the stresses are known for each loading condition and the strain was calculated from the weighted average of the displacements of the nodes of the line $\overline{EF}$ and the initial length $\overline{AE}$, Fig. 4.

To check the reproducibility of the method of calculations, with the present modifications and procedure, and also to find out the limit of the strain up to which calculations could be performed with minimum error, the whole mesh in Fig. 1 was made α and the calculations

were performed. It was found that the calculated α curve closely followed the input α curve upto a strain of 0.05, after which the calculated α curve rose sharply above the input α curve, not shown here. Hence, all the calculations were restricted to a total strain 0.05 or less in the $\alpha-\beta$ alloys considered. It should be noted that even though the average strains in the $\alpha-\beta$ alloys, Figs. 7 to 10 and 12, are lower than 0.05 strain, there are instances, in particular for stress levels 896 MPa (130 KSi) and 965 MPa (140 KSi) of the configuration of Fig. 1 and, for the stress level 965 MPa (140 KSi) of the configuration of Fig. 2, for which the average strain in the α phase is slightly higher than 0.05. Since the volume percent of α in these configurations, Figs. 1 and 2, is only 16.3%, the errors arising from this strain would have only a small effect on the calculated $\alpha-\beta$ stress-strain curves, Fig. 8.

To ascertain the effect of particle size on the calculated $\sigma-\varepsilon$ curve, the particle size was varied as shown in Figs. 1 to 3, while keeping the 16.3 vol. % α constant.

The mesh used to calculate the effect of matrix is shown in Fig. 4. For this calculation only the area of the mesh ABFE was considered and the area EFDC was made as the stronger phase, β, so that it served as approximately a rigid body, with minimum differences in the displacements of the nodes along the edge $\overline{CD}$. This had to be done because the multipoint constraint described above was not incorporated for this calculation, as mentioned above. Within the area ABFE, the volume fractions of α and β are 0.50. In one calculation the shaded phase, Fig. 4, was made α, the particles and the unshaded phase β as the matrix. In the comparison calculation the

designations were reversed. In this process of interchanging the two phases, nothing else was changed, and hence the difference between the two calculated curves, Fig. 9, gives the effect of the matrix.

Calculations were also made for the volume percents of α of 41, 63 and 80 and for the configurations of the particle sizes similar to Figs. 1 and 3. However, the meshes used for the calculations for the 41 and 63 volume percents α are not shown here. When the volume percent of α was 80, the β was in the form of particles and the configurations of β for this α - β alloy are shown in Figs. 5 and 6.

The calculations, made with the minor phase in the form of triangles, as in Fig. 3, are compared with the experimentally determined curves for all four α - β alloys in Fig. 12. All the four α-β alloys were annealed for 200 hrs. at 700^{o}C (973^{o}K), and tensile tests were conducted on a Tinius Olsen testing machine with 2.54 cm (1 inch) standard gauge length specimens.

RESULTS AND DISCUSSION

A. Comparison with the Previous Work (12):

The calculated curve, obtained with the mesh of Fig. 1 for the 16.3 vol. % α alloy is shown in Fig. 7. This stress-strain curve lay above the calculated curve of previous work (12), Fig. 7, for the same volume percent of α. The flow stress difference between the two curves at a true strain of 0.015 is 79 MPa (11.5 KSI). Part of this difference obviously is due to the difference in input stress-strain curves of the α and β phases for the two calculations. Part of this difference could also be due to the size and shape of the α particles used in the mesh of Fig. 1 and in the mesh of the previous

work (12), even though the interface area/unit volume is not significantly different.

Even though the calculated curve of the present work is above the calculated curve of the previous work (12), it is, nevertheless considerably below the experimental curve, shown in Fig. 7. The flow stress difference between these two curves at a strain of 0.015 is about 104 MPa (15KSI). If one recognizes that in the mesh of Fig. 1. $\overline{AB}$ represents the diameter of the specimen, 6.35 mm, then the particle size in the mesh is very much larger than the particle size of the test specimen. Thus it appeared desirable to ascertain whether the discrepancy between calculated and experimental results was related to particle size.

B. Effect of Particle Size:

The meshes used to calculate the effect of particle size for a constant 16.3 vol. % α are shown in Figs. 1 to 3 and the corresponding calculated stress-strain curves are shown in Fig. 8. It can be seen that, as the particle size gets smaller, the calculated stress-strain curve tends to be higher, Fig. 8. The variation in interface area/unit volume is 3.5 times when the particle size varied from coarse, Fig. 1 to fine, Fig. 3. The flow stress, for a given strain, for the fine α particle configuration is higher than that for the coarse α particles, because the strain differences between the α and β phases are smaller for the fine than for the coarse particles. The smaller strain difference means that the β has also undergone considerable larger strains which, in turn, means a higher flow stress, because β is stronger than α.

The difference in the flow stress between the calculated curves, Fig. 8, starts to be different, almost from the point of proportional limit, 414 MPa (60KSi). Thereupon the difference between the flow stresses, for specific strains, tends to be increasingly different up to a strain of 0.0125, at which point the maximum difference occurs. This maximum difference between the coarse and fine particles, upper and lower curves in Fig. 8, is about 69 MPa (10 KSi) and this difference remains fairly constant up to a strain of 0.0262. Comparison of the calculated curves, Fig. 8 for coarse, Fig. 1, and medium size, Fig. 2, α particles indicates that the difference in the flow stress tends to be reduced beyond the strain 0.0262 and the flow stresses are very close at a strain 0.035.

An attempt has been made to determine what size of the α particles in the mesh needs to be used so that the calculated curve closely approaches the experimental curve. This was done by extrapolating the flow stress vs. the particle size** for specific total strains to the flow stress of the experimental curve, Fig. 7. It was found that this size depends on the magnitude of the total strain. The extrapolated particle size at a total strain of 0.0075 was 30 μm and 150 μm at a total strain of 0.025, these sizes are, respectively, 1/9 and 3/5 of the particle size of Fig. 3. At intermediate total strains, the particle sizes were intermediate also. It is to be noted that the size of the α particles in the actual material was 4.4 μm. Therefore, these results suggest that at strains above 0.025 the particle size (or the interface

---

** If the line $\overline{AB}$ in Figs. 1 to 3 is considered as the diameter, of the specimen, then the equivalent particle sizes in these figures are 906, 453 and 259 μm, respectively.

area/unit volume) does not have much influence on the flow stress, whereas at lower strains particle size does influence the flow stress. Some support for this line of reasoning comes from the work of Margolin and Stanescu (20). These workers showed for polycrystalline material, that the difference in the strength levels between the grain boundary zone and grain interior is largest at low plastic strains and decreased with increasing plastic strains until at 2% the two regions had the same flow stress.

As will be shown later, Fig. 12, the calculated curve with fine α particles is close to the experimental curve. Therefore, these calculations underline the need to use fine α particles, or a large area of the actual microstructure to represent the α particles in the actual α - β alloys, a need not expressed in previous investigations (8-10,12).

C. Effect of Matrix:

The calculated stress-strain curves are shown in Fig. 9. It can be seen that the curve with β as matrix lies above the the curve with α as matrix. This behavior is expected, since β is stronger than α. Since coarse particles were used for these calculations it is to be expected that both curves would be raised with finer particle sizes. However, as can be seen from a comparison of Figs. 8 and 10, the β matrix curve would be expected to be raised more than the α matrix curve. Comparison of the two curves in Fig. 9 indicates that the flow stress differences, at a given true strain, starts to be significantly different only after about 0.2% plastic strain, unlike the effect of particle size where the flow stress differences started to be significant from the proportional limit onward, Fig. 8.

D. Effect of Volume Fraction:

Calculations for coarse and fine particle sizes, comparable to Figs. 1 and 3 were also made for 41, 63, and 80 vol. % α alloys. The calculated stress-strain curves for the 80 vol. % α alloy are shown in Fig. 10. Figure 10 reveals that the difference between the calculated curves starts to be significant right from the proportional limit, as was found earlier for the 16.3 vol.% α alloy, Fig. 8, and reaches a maximum which is 48 MPa (7 KSI) at a strain 0.0232.

The behavior of the calculated curves for the coarse and fine second phase particles for the 63 and 41 vol.% α alloys were in between that of the 80, Fig. 10, and 16.3, Fig. 8. vol.% α alloys and hence are not shown here. However, the 0.2% and 0.4% offset YS differences between the coarse and fine second phase particle calculated curves, for all the four α-β alloys are given in Fig. 11. It indicates that the particle size effects are more important for the YS determination in the range of 35 to 90 volume percent β.

E. Comparison of Calculated and Experimental Curves:

The calculated and experimental stress-strain curves for the four α-β alloys are presented in Fig. 12. The calculated curves are for fine second phase particles. It can be seen that for all the alloys, the FEM calculated curves predict deviation from elastic behavior at a lower stress than the experimental curves. In addition, the calculated flow stresses at strains, just after the proportional limits of the experimental curves, are lower than the experimental flow stresses. For example, for the alloys 2, 3, 4 and 5 at the strains 0.0039, 0.005, 0.0063 and 0.0101, the differences are 48 MPa (7 KSi), 79 MPa (11.5 KSi), 69 MPa (10 KSi) and 48 MPa (7 KSi), respectively.

These are the maximum differences between the flow stresses of the calculated and experimental curves and at higher strain levels, the differences are reduced. These calculations are consistent with the FEM calculation of Fischmeister and Karlsson (10) where it was observed that, for a ferrite + martensite steel, the maximum difference between the calculated and experimental results occur at the very beginning of the plastic deformation.

As mentioned earlier, the particle sizes of Figs. 3 and 6 are very much coarser than the actual particle sizes of the alloys. Consequently, if still finer particle sizes were used, it would be reasonable to expect that the calculated curves would approach the experimental curves more closely still. Further support for this view comes from the fact that of all the four alloys, mentioned above, the maximum difference of 79 MPa (11.5 KSi) between calculated and experimental curves occurred for alloy 3, which also was found experimentally to have the highest interface area/unit volume. The differences in the calculated and experimental curves, in general, are very small at higher strains, Fig. 12.

Fig. 12 shows that at the larger plastic strains, the calculated curve lies above the experimental curve for alloy 2, whereas for alloys 3, 4 and 5 alloys the calculated curves lie below the experimental curves. As earlier results on the matrix effect for a 50 vol.% α revealed, when β was the matrix, the calculated stress-strain curve was higher than when α was the matrix. The β particles arranged in the mesh of Fig. 6 for alloy 2 tend to be more continuous than the β particles in the actual material. Thus, the calculated curve would be expected to lie above the experimental curve at the larger strains, as

shown in Fig. 12. For the alloys, 3, 4 and 5, the α particle arrangement tend to be more continuous than α in the actual materials and hence lower calculated curves than the experimental curves would be expected. This is also seen in Fig. 12. With the exceptions noted, it appears that the FEM satisfactorily predicts the stress-strain behavior of the two ductile phase alloys, from the stress-strain behavior of the component phases and volume fractions.

It should be noted, however, that in addition to the 0.05 strain limitation mentioned earlier, the present use of the FEM has not considered the anisotropy of behavior of the alpha and beta phases, either elastically or plastically. No distinction has been made between slip behavior in equiaxed and Widmanstätten alpha. Furthermore the presumption of compatibility at α-β interfaces rules out the possibility of a breakdown of the compatibility which would lead either to void formation or cracking which can occur at very low strains (21).

CONCLUSIONS

1 By using NASTRAN (18) computer program and stress-strain curves of the α and β phases of Ti-Mn alloys, the Finite Element Method (FEM) has been successfully employed to calculate the effect of particle size, matrix and volume fraction on the stress-strain relations of two phase α-β titanium alloys.

2) Calculations of the stress-strain curve of a 16 volume percent α alloy were carried out for three particle sizes. As the particle size decreased, the calculated curve approached the experimental curve and was close to it for the smallest particle size used, 260 μm. Calculations showed that the particle size which would

produce the experimental curve depended upon the strain, and the smallest particle sizes were required for the smallest strain. In general deviation between calculated and experimental curves for the 80, 63, 41 and 16.3 volume percent α alloys were largest at the onset of plastic deformation and diminished with increasing strain. Additional calculations showed that the particle size effect was strongest in the region 35-90 volume percent β.

3) The matrix effect was determined by using a mesh in which the α and β phases were present in equal amounts. The properties of the matrix phase were alternately assigned to α and β. It was found, as anticipated, that when the stronger phase, β, was matrix, the stress-strain curve reached higher stresses. Because the particle size used was coarse, it is quite likely that the strengthening effect of the β matrix phase was not fully realized. The small differences between calculated and experimental curves were found to be consistent with the "degree of matricity" of the particle phase as well as the particle size.

ACKNOWLEDGMENTS

This work was supported by the Office of Naval Research on Contract N-00014-75-C-0793. The authors wish to express their appreciation to Dr. Bruce MacDonald for his continued interest and encouragement.

REFERENCES

1. J.E. Dorn and C.D. Starr, Relations of Properties to Microstructure, American Society for Metals, Ohio, 1954, p. 71.

2. R.G. Davies: Met. Trans. 9A (1978) p.41.

3. R.G. Davies: ibid. p.451.

4. R.G. Davies: ibid. p.671.

5. S.T. Mileiko: J. Mater. Sci., 1969, vol. 4, p.974.

6. G. Garmong and R.B. Thompson: Met. Trans., 1973, vol. 4, p.863.

7. Y. Tomota, K. Kuroki, T. Mori, and I. Tamura: Mat. Sci. Eng., 24 (1976) p.85.

8. H. Fischmeister, J.-O. Hjälmered, B. Karlsson, G. Linden and B. Sundstrom: Proc. Third Int. Conf. Strength of Metals and Alloys, Inst. of Metals and Iron and Steel Inst., Cambridge and London, 1973, vol. 1, p. 621.

9. B. Karlsson and B.O. Sundstrom: Mat. Sci. Eng. 16 (1974) p.161.

10. H. Fischmeister and B. Karlsson: Z. Metallkunde, 68 (May 1977) p. 311.

11. O.C. Zienkiewicz, The Finite Element Method in Engineering Science, McGraw-Hill, New York, 1971.

12. J. Jinoch, S. Ankem and H. Margolin: Mat. Sci. Eng. 34 (1978) p. 203.

13. S. Ankem and H. Margolin: Metall. Trans., 8A (1977) p.1320.

14. C.G. Rhodes and J.C. Williams: Metall. Trans., 6A (1975) 1670.

15. C.G. Rhodes and J.C. Williams: ibid. p. 2103.

16. H. Margolin, E. Levine and M. Young: Metall. Trans., 8A (1977) p. 373.

17. C.G. Rhodes and N.E. Paton: Final Report submitted to Office of Naval Research (1979). Contract No. N00014-76-C-0598.

18. C.W. McCormick (ed.), NASTRAN Users Manual Level 15.5, May 1973, Document NASA ST[(222)01], published by National Aeronautics and Space Administration, Washington, DC.

19. R.L. Jones and H. Conrad, Trans. Metall. Soc. AIME, 245 (1969) 779.

20. H. Margolin and M.S. Stanescu: Acta Met. Vol. 23 (1975) p. 1411.

21. Y. Mahajan and H. Margolin: Metall. Trans. A, vol. 8A (1978) p. 427.

FIGURES

Fig. 1. Mesh 1, Coarse α particles (16.3 vol. %), shaded, in a β matrix, unshaded.

Fig. 2. Mesh 2, Medium size α particles (16.3 vol. %), shaded, in the β matrix, unshaded.

Fig. 3. Mesh 3, Fine α particles (16.3 vol. %), shaded, in the β matrix, unshaded.

Fig. 4. Mesh 4, Particles Phase shaded and matrix phase unshaded. Particles and Matrix in equal amounts within the area of the mesh ABFE.

Fig. 5. Mesh 5, Coarse β particles (20 vol. %), shaded, in the α matrix, unshaded.

Fig. 6. Mesh 6, Fine β particles (20 vol. %), shaded, in the α matrix unshaded.

Fig. 7. The stress-strain curves of the α and β phases used for the FEM calculations, calculated curve for a 16.3 vol. % α alloy with coarse α particles with Mesh 1 of Fig. 1, FEM calculated curve for a 16.6 vol. % α alloy from the previous work (12) and, experimentally determined stress-strain curve for a similar (~ 17) vol. % α alloy.

Fig. 8. FEM calculated stress-strain curves for a 16.3 vol. % α alloy with three different α particle sizes, Figs. 1 to 3.

Fig. 9. FEM calculated stress-strain curves for a 50 vol. % α-β alloy, Fig. 4, one with α and β alternately as matrix.

Fig. 10. FEM calculated stress-strain curves for an 80 vol. % α alloy with two different particle sizes of β, Figs. 5 and 6.

Fig. 11. 0.2 and 0.4% offset yield strength differences between the coarse and fine second phase particles vs. the volume percent of β.

Fig. 12. Comparison of the FEM calculated stress-strain curves, with fine second phase particles, with corresponding experimental stress-strain curves.

FIGURE 1

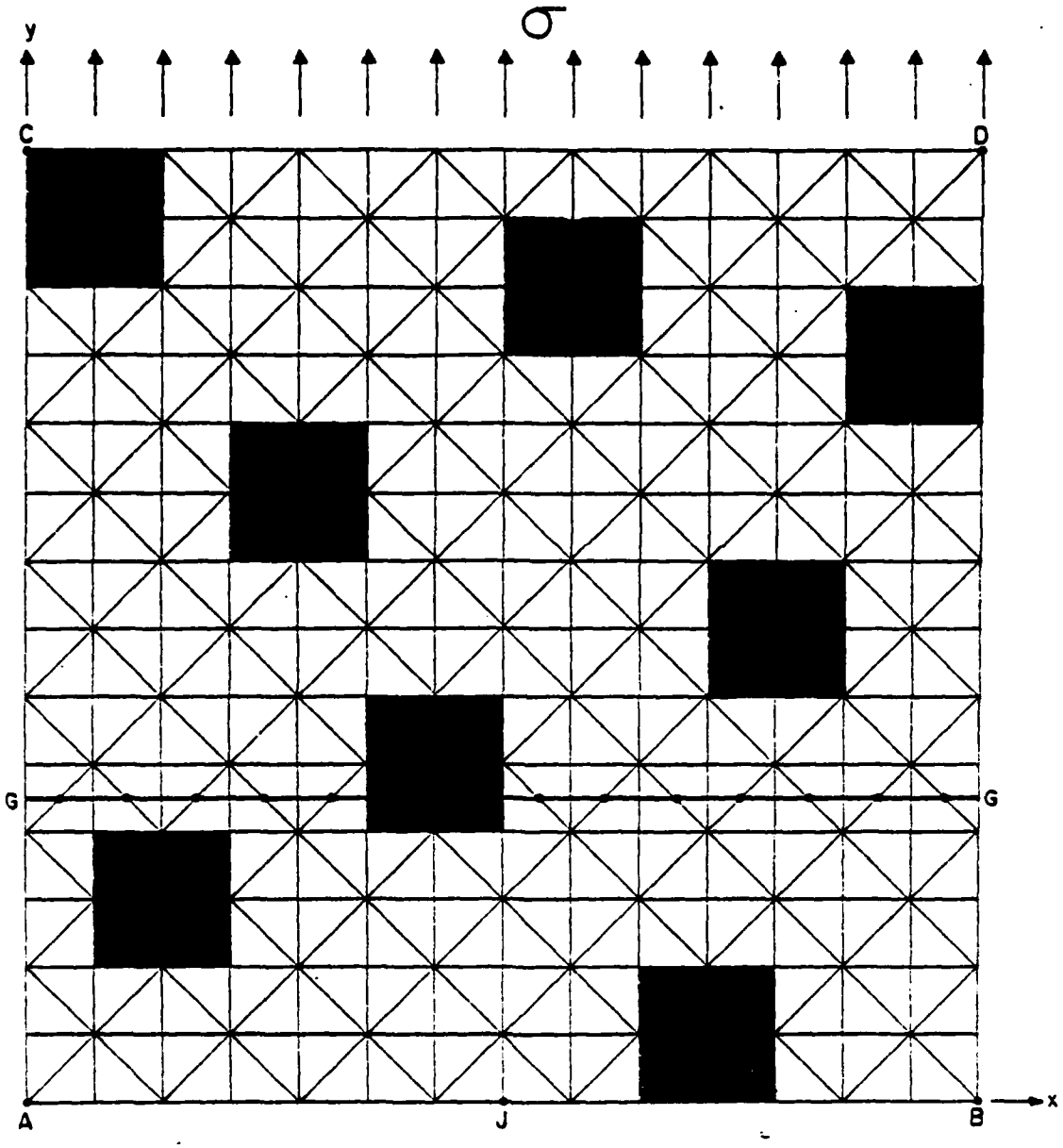

FIGURE 2

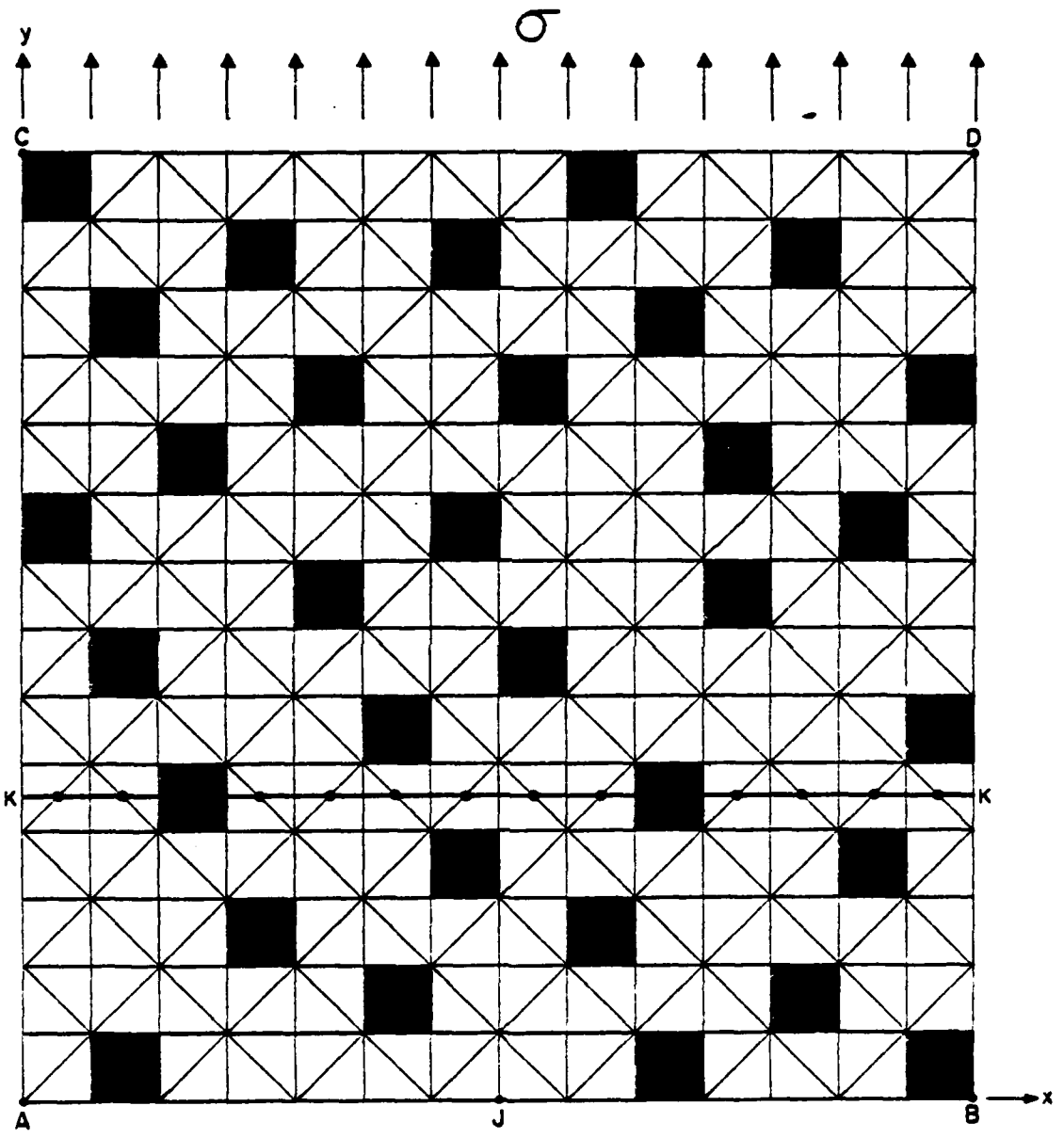

FIGURE 3

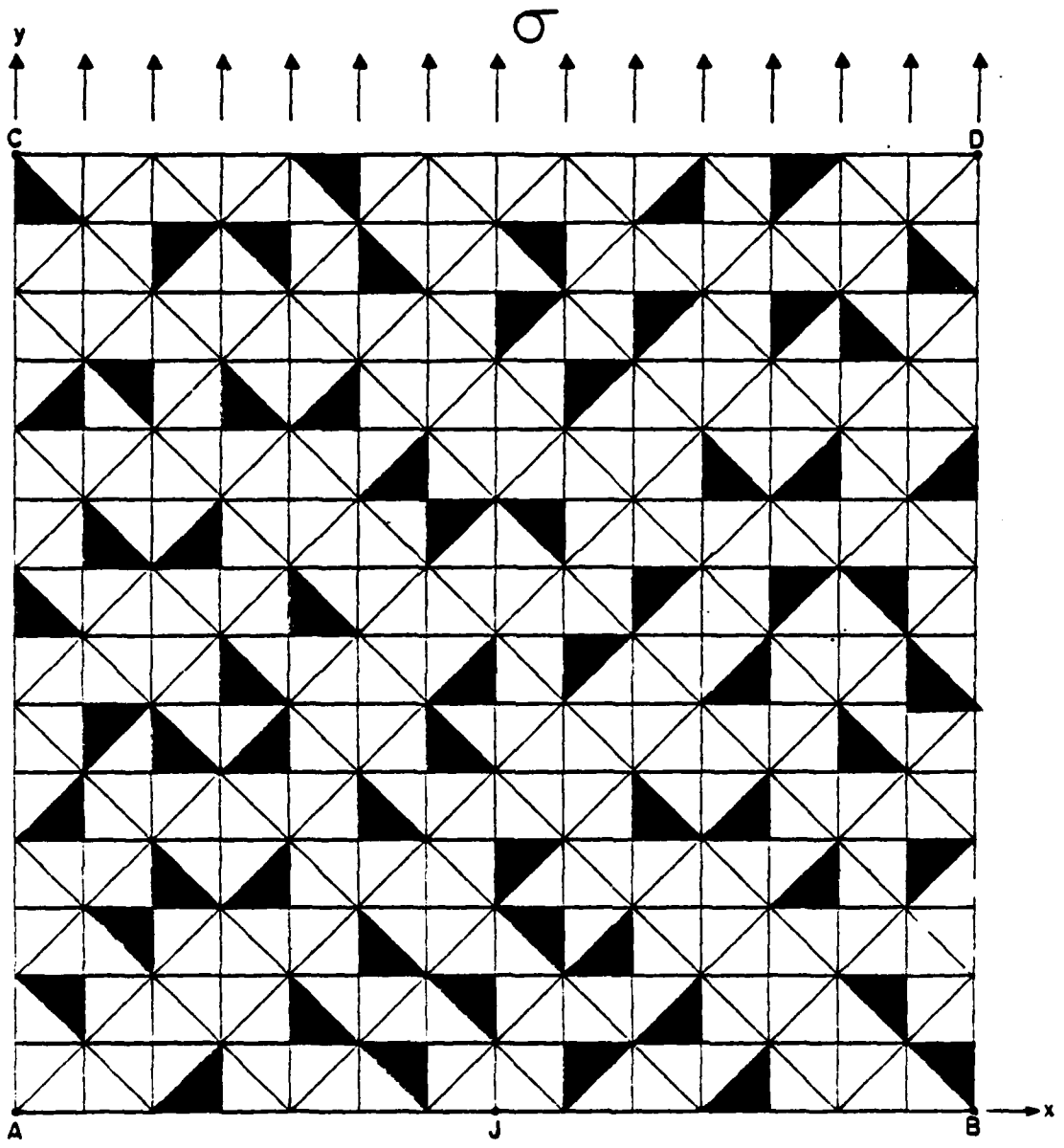

FIGURE 4

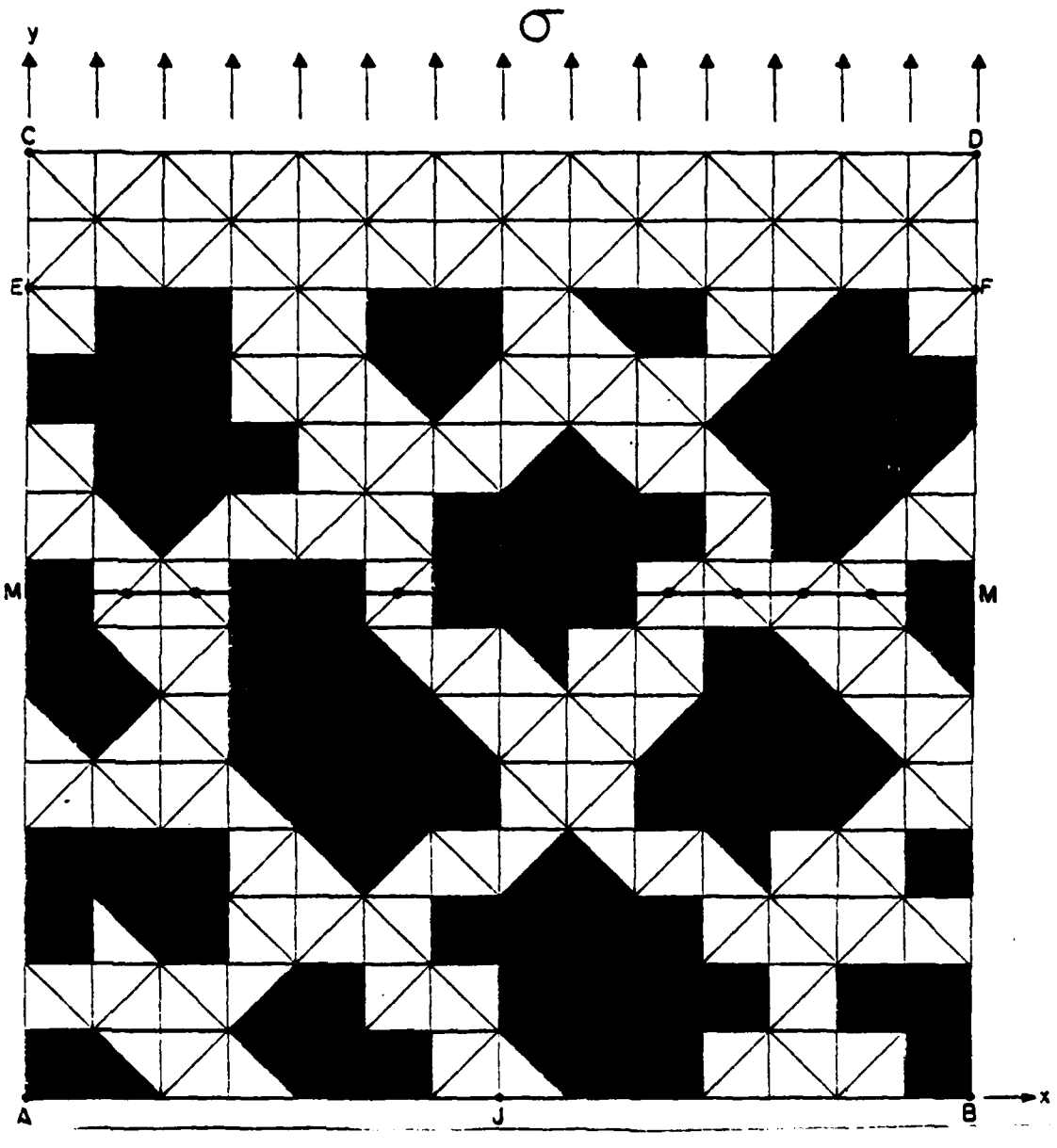

FIGURE 5

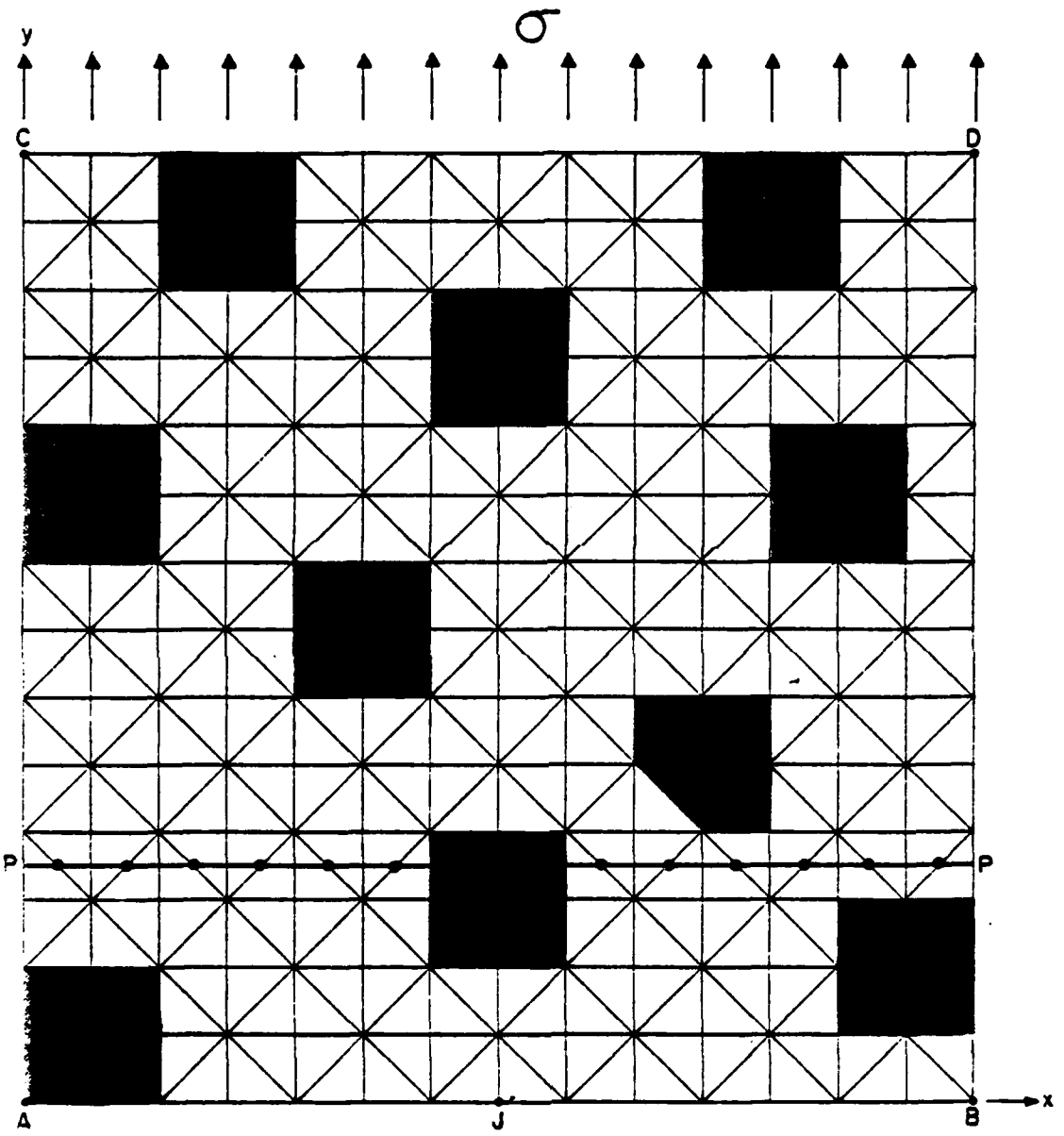

FIGURE 6

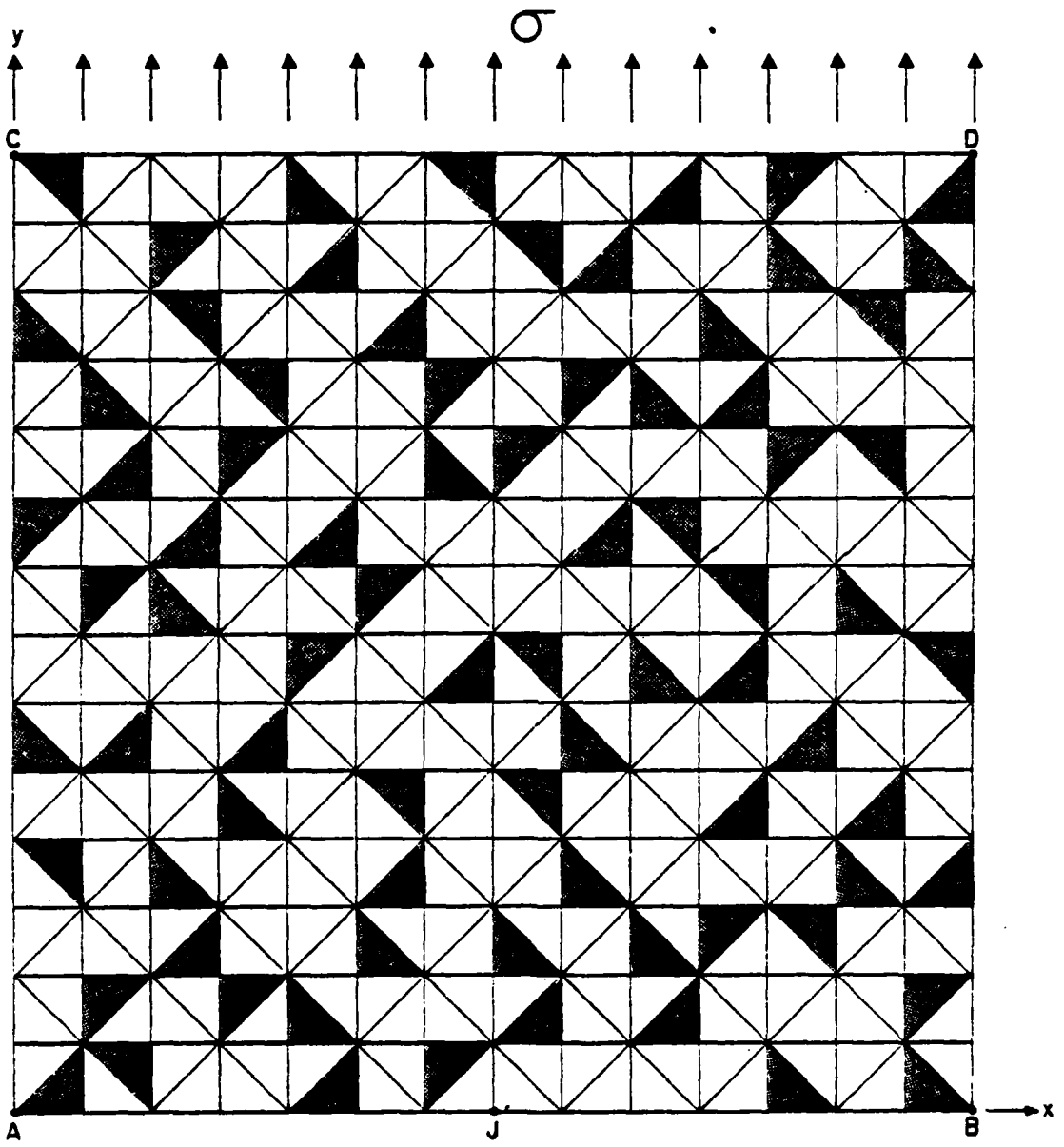

FIGURE 7

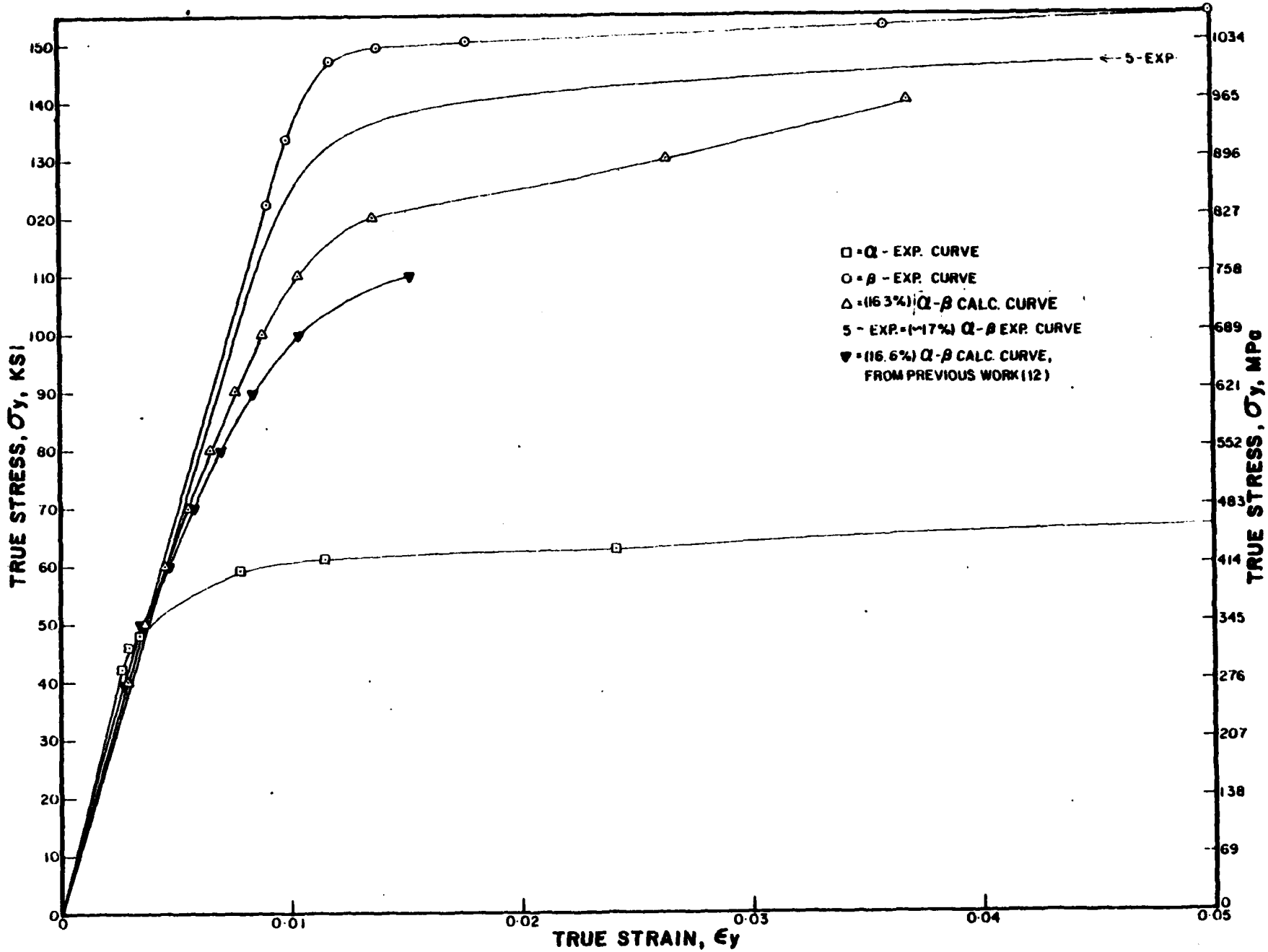
TRUE STRESS, σy, KSI
TRUE STRESS, σy, MPa
TRUE STRAIN, εy
0
10
20
30
40
50
60
70
80
90
100
110
020
130
140
150
0·01
0·02
0·03
0·04
0·05
69
138
207
276
345
414
483
552
621
689
758
827
896
965
1034
← 5 - EXP.
□ = α - EXP. CURVE
○ = β - EXP. CURVE
△ = (16.3%) α-β CALC. CURVE
5 - EXP. = (~17%) α-β EXP. CURVE
▼ = (16.6%) α-β CALC. CURVE, FROM PREVIOUS WORK (12)

FIGURE 8

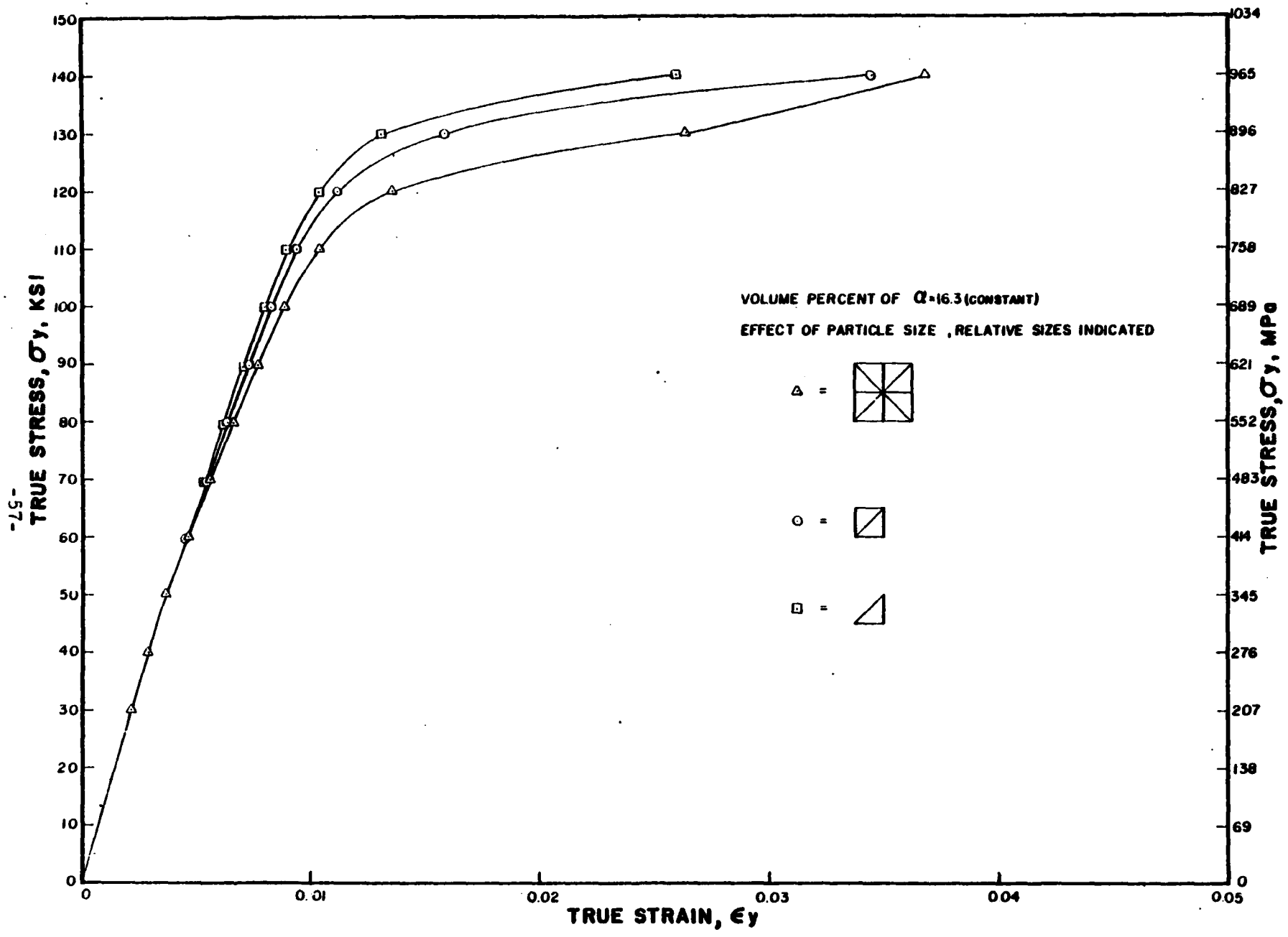
TRUE STRESS, σy, KSI
TRUE STRESS, σy, MPa
TRUE STRAIN, εy
VOLUME PERCENT OF α=16.3 (CONSTANT)
EFFECT OF PARTICLE SIZE, RELATIVE SIZES INDICATED
Δ =
O =
□ =
0
10
20
30
40
50
60
70
80
90
100
110
120
130
140
150
0
69
138
207
276
345
414
483
552
621
689
758
827
896
965
1034
0
0.01
0.02
0.03
0.04
0.05

FIGURE 9

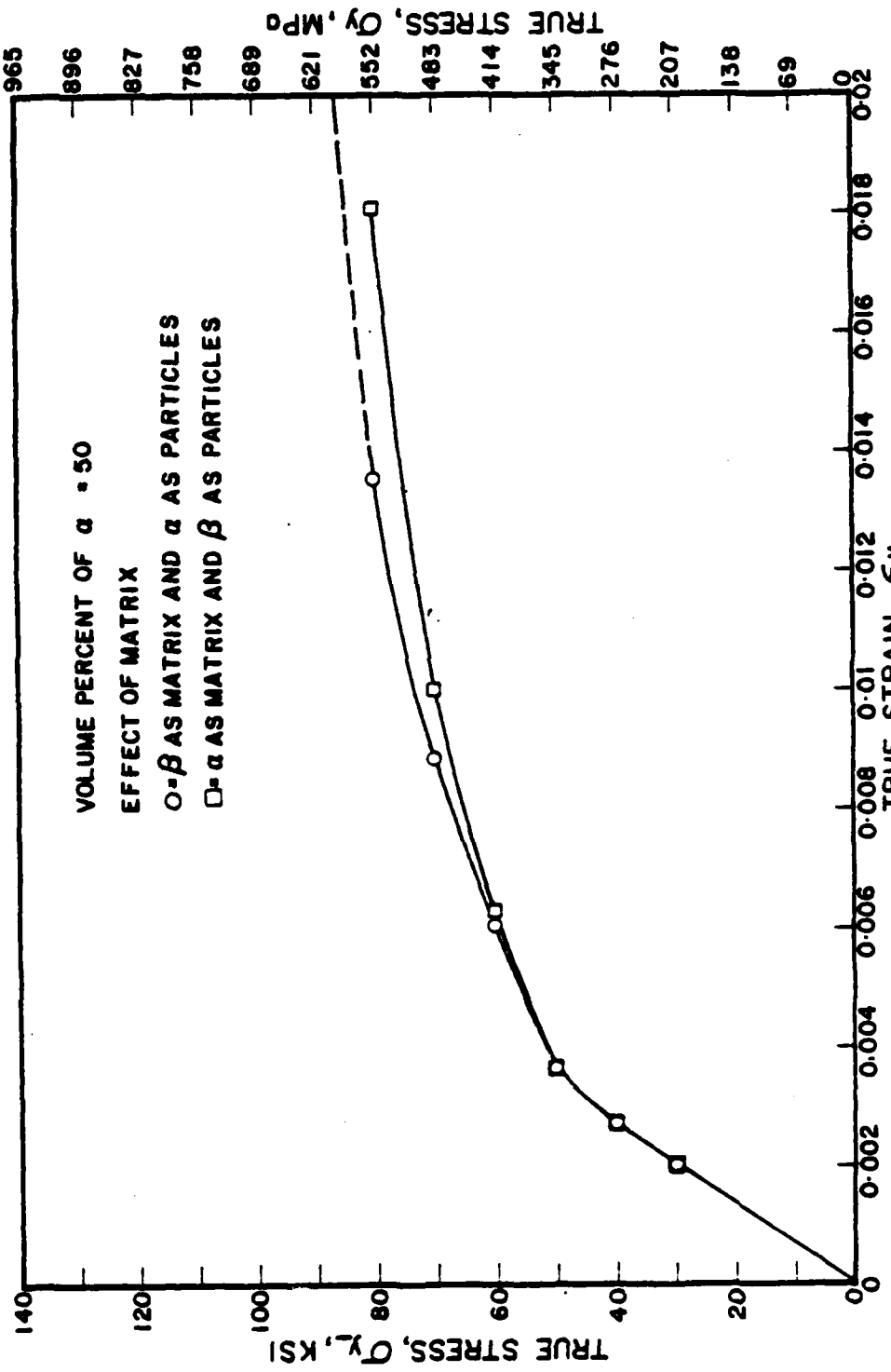
VOLUME PERCENT OF α = 50
EFFECT OF MATRIX
○-β AS MATRIX AND α AS PARTICLES
□-α AS MATRIX AND β AS PARTICLES
TRUE STRESS, σy, KSI
TRUE STRESS, σy, MPa
TRUE STRAIN, εy
0
20
40
60
80
100
120
140
0
69
138
207
276
345
414
483
552
621
689
758
827
896
965
0·002
0·004
0·006
0·008
0·01
0·012
0·014
0·016
0·018
0·02

FIGURE 10

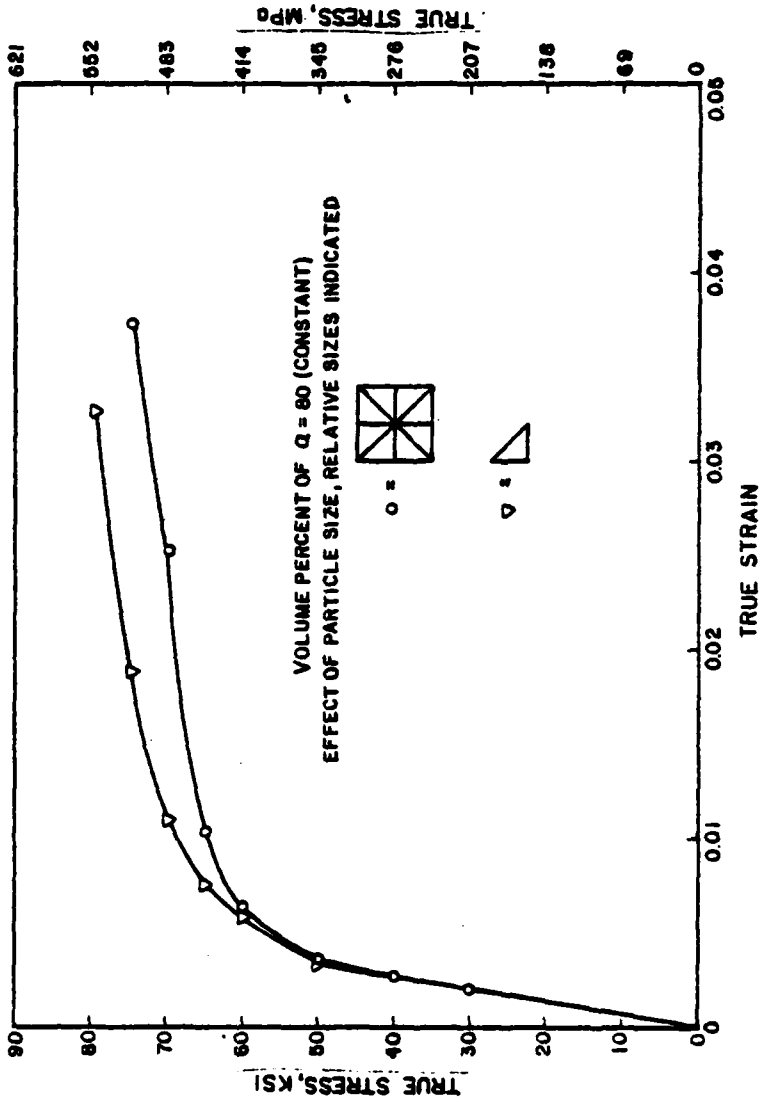
TRUE STRESS, MPa
621
552
483
414
345
276
207
138
69
0
0.06
0.04
0.03
0.02
0.01
0
TRUE STRAIN
VOLUME PERCENT OF α = 80 (CONSTANT)
EFFECT OF PARTICLE SIZE, RELATIVE SIZES INDICATED
o =
▽ =
TRUE STRESS, KSI
90
80
70
60
50
40
30
20
10
0

FIGURE 11

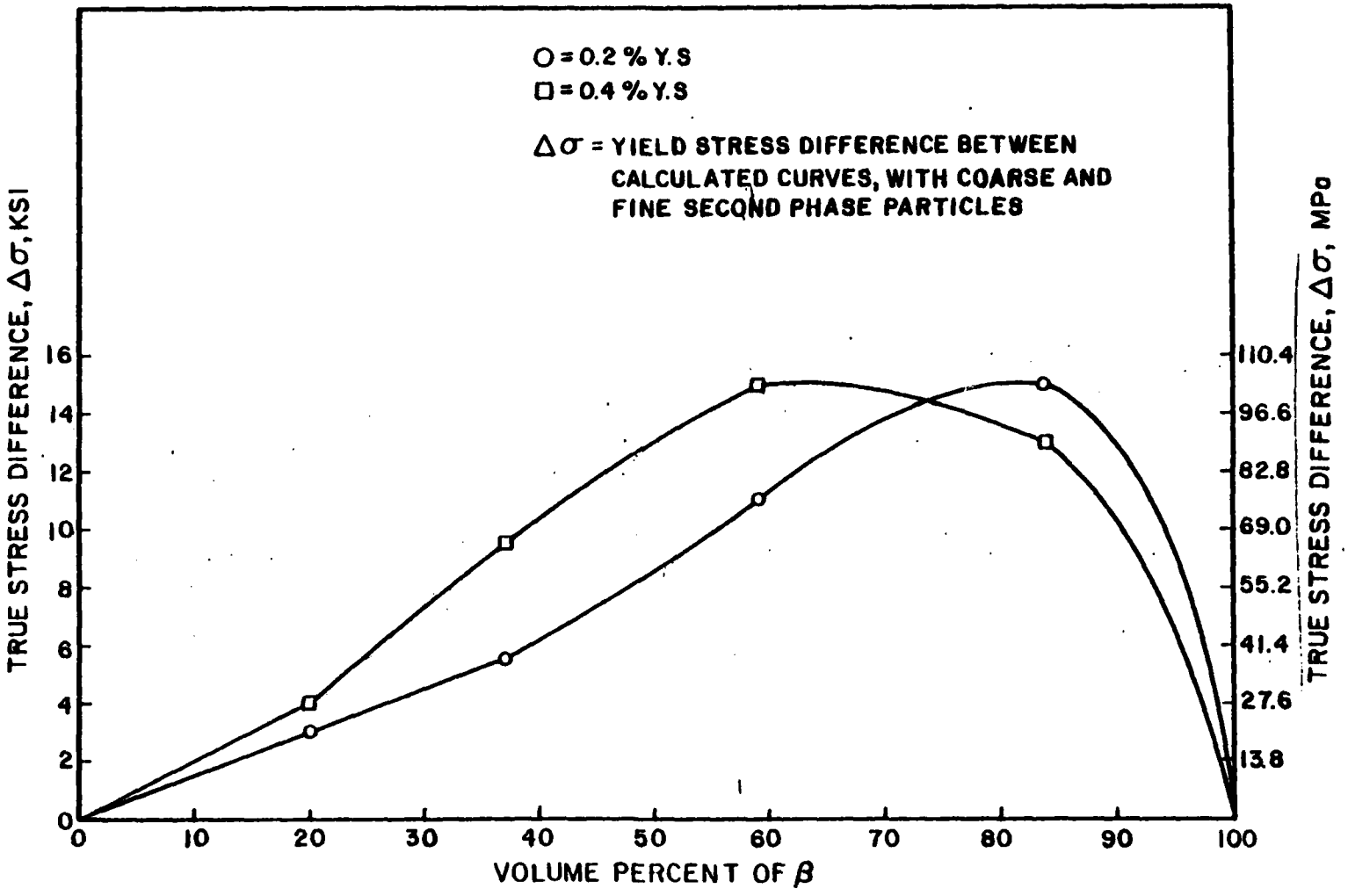
O = 0.2 % Y.S
□ = 0.4 % Y.S
Δσ = YIELD STRESS DIFFERENCE BETWEEN CALCULATED CURVES, WITH COARSE AND FINE SECOND PHASE PARTICLES
TRUE STRESS DIFFERENCE, Δσ, KSI
TRUE STRESS DIFFERENCE, Δσ, MPa
0
2
4
6
8
10
12
14
16
13.8
27.6
41.4
55.2
69.0
82.8
96.6
110.4
0
10
20
30
40
50
60
70
80
90
100
VOLUME PERCENT OF β

FIGURE 12

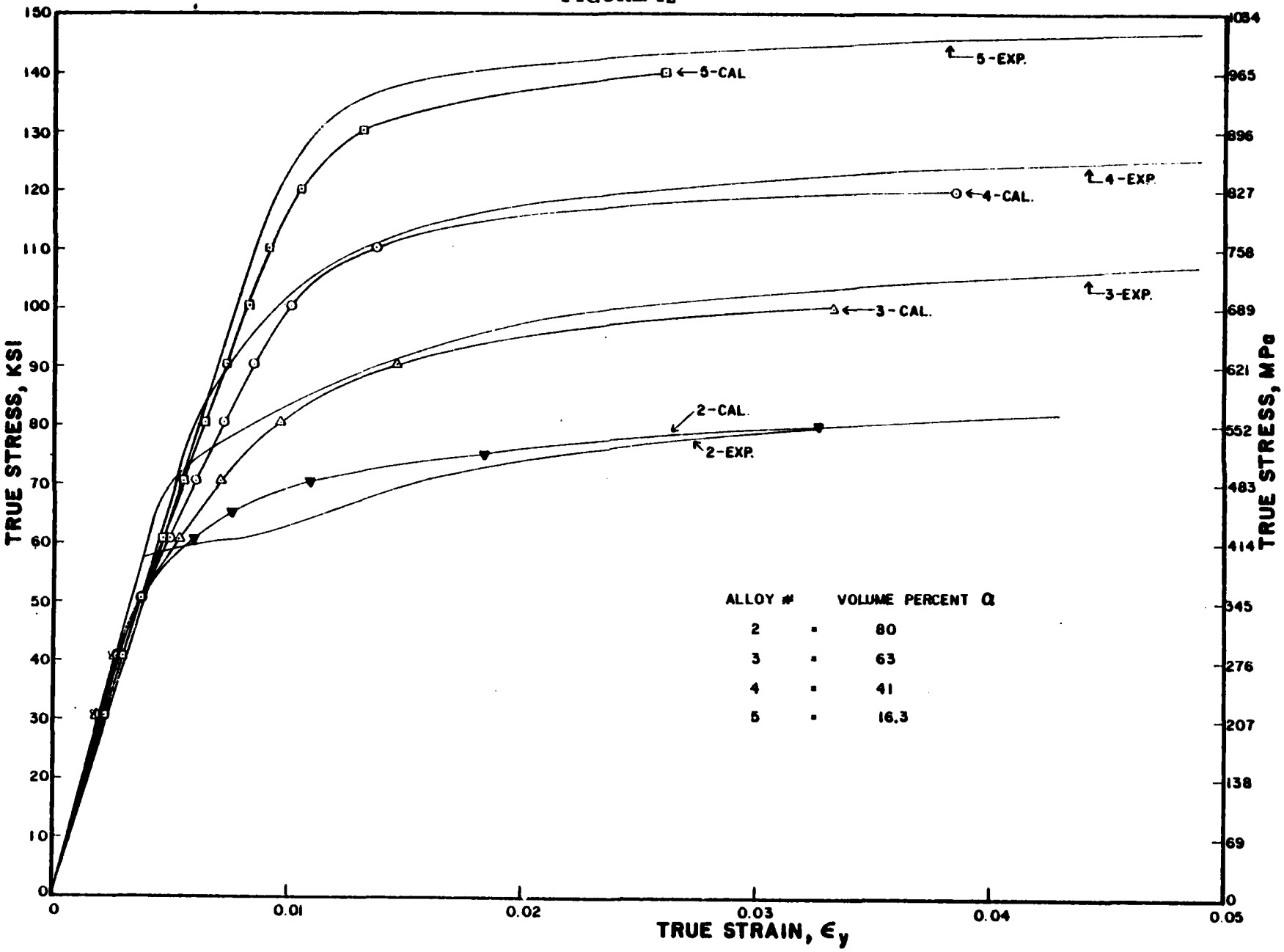
TRUE STRESS, KSI
TRUE STRESS, MPa
TRUE STRAIN, ϵ_y
5-EXP.
5-CAL
4-EXP.
4-CAL.
3-EXP.
3-CAL.
2-CAL.
2-EXP.
ALLOY # VOLUME PERCENT α
2 = 80
3 = 63
4 = 41
5 = 16.3

BASIC DISTRIBUTION LIST

Technical and Summary Reports November 1979

Organization	Copies
Defense Documentation Center Cameron Station Alexandria, VA 22314	12
Office of Naval Research Department of the Navy 800 N. Quincy Street Arlington, VA 22217 ATTN: Code 471	1
Code 470	1
Commanding Officer Office of Naval Research Branch Office Building 114, Section D 666 Summer Street Boston, MA 02210	1
Commanding Officer Office of Naval Research Branch Office 536 South Clark Street Chicago, IL 60605	1
Office of Naval Research San Francisco Area Office One Hallidie Plaza Suite 601 San Francisco, CA 94102	1
Naval Research Laboratory Washington, DC 20375 ATTN: Codes 6000	1
6100	1
6300	1
2627	1
Naval Air Development Center Code 606 Warminster, PA 18974 ATTN: Mr. F. S. Williams	1

Organization	Copies
Naval Air Propulsion Test Center Trenton, NJ 08628 ATTN: Library	1
Naval Construction Batallion Civil Engineering Laboratory Port Hueneme, CA 93043 ATTN: Materials Division	1
Naval Electronics Laboratory San Diego, CA 92152 ATTN: Electron Materials Sciences Division	1
Naval Missile Center Materials Consultant Code 3312-1 Point Mugu, CA 92041	1
Commanding Officer Naval Surface Weapons Center White Oak Laboratory Silver Spring, MD 20910 ATTN: Library	1
Commander David W. Taylor Naval Ship Research and Development Center Bethesda, MD 20084	1
Naval Oceans Systems Center San Diego, CA 92132 ATTN: Library	1
Naval Underwater System Center Newport, RI 02840 ATTN: Library	1
Naval Postgraduate School Monterey, CA 93940 ATTN: Mechanical Engineering Department	1
Naval Weapons Center China Lake, CA 93555 ATTN: Library	1

BASIC DISTRIBUTION LIST (cont'd)

Organization	Copies
Naval Air Systems Command Washington, DC 20360 ATTN: Codes 52031	1
52032	1
Naval Sea System Command Washington, DC 20362 ATTN: Code 05R	1
Naval Facilities Engineering Command Alexandria, VA 22331 ATTN: Code 03	1
Scientific Advisor Commandant of the Marine Corps Washington, DC 20380 ATTN: Code AX	1
Army Research Office P. O. Box 12211 Triangle Park, NC 27709 ATTN: Metallurgy & Ceramics Program	1
Army Materials and Mechanics Research Center Watertown, MA 02172 ATTN: Research Programs Office	
Air Force Office of Scientific Research/NE Building 410 Bolling Air Force Base Washington, DC 20332 ATTN: Chemical Science Directorate	1
Electronics & Materials Sciences Directorate	1
Air Force Materials Laboratory Wright-Patterson AFB Dayton, OH 45433	1
Library Building 50, Room 134 Lawrence Radiation Laboratory Berkeley, CA	1
NASA Headquarters Washington, DC 20546 ATTN: Code RRM	1

Organization	Copies
NASA Lewis Research Center 21000 Brookpark Road Cleveland, OH 44135 ATTN: Library	1
National Bureau of Standards Washington, DC 20234 ATTN: Metals Science and Standards Division	1
Ceramics Glass and Solid State Science Division	1
Fracture and Deformation Division	1
Director Applied Physics Laboratory University of Washington 1013 Northeast Forthieth Street Seattle, WA 98105	1
Defense Metals and Ceramics Information Center Battelle Memorial Institute 505 King Avenue Columbus, OH 43201	1
Metals and Ceramics Division Oak Ridge National Laboratory P. O. Box X Oak Ridge, TN 37380	1
Los Alamos Scientific Laboratory P. O. Box 1663 Los Alamos, NM 87544 ATTN: Report Librarian	1
Argonne National Laboratory Metallurgy Division P. O. Box 229 Lemont, IL 60439	1
Brookhaven National Laboratory Technical Information Division Upton, Long Island New York 11973 ATTN: Research Library	1
Office of Naval Research Branch Office 1030 East Green Street Pasadena, CA 91106	1

M
January 1979

SUPPLEMENTARY DISTRIBUTION LIST

Technical and Summary Reports

Professor G. S. Ansell
Rensselaer Polytechnic Institute
Dept. of Metallurgical Engineering
Troy, New York 02181

Professor H. K. Birnbaum
University of Illinois
Department of Metallurgy
Urbana, Illinois 61801

Dr. E. M. Breinan
United Technology Corporation
United Technology Research Laboratories
East Hartford, Connecticut 06108

Professor H. D. Brody
University of Pittsburgh
School of Engineering
Pittsburgh, Pennsylvania 15213

Mr. R. Morante
General Dynamics
Electric Boat Division
Eastern Point Road
Groton, Connecticut 06340

Professor J. B. Cohen
Northwestern University
Dept. of Material Sciences
Evanston, Illinois 60201

Professor M. Cohen
Massachusetts Institute of Technology
Department of Metallurgy
Cambridge, Massachusetts 02139

Professor Thomas W. Eagar
Massachusetts Institute of Technology
Department of Materials Science
and Engineering
Cambridge, Massachusetts 02139

Professor B. C. Giessen
Northeastern University
Department of Chemistry
Boston, Massachusetts 02115

Professor D. G. Howden
Ohio State University
Dept. of Welding Engineering
190 West 19th Avenue
Columbus, Ohio 43210

Dr. C. S. Kortovich
TRW, Inc.
23555 Euclid Avenue
Cleveland, Ohio 44117

Professor D. A. Koss
Michigan Technological University
College of Metallurgical Engineering
Houghton, Michigan 49931

Professor A. Lawley
Drexel University
Dept. of Metallurgical Engineering
Philadelphia, Pennsylvania 19104

Professor Harris Marcus
The University of Texas at Austin
College of Engineering
Austin, Texas 78712

Dr. H. Margolin
Polytechnic Institute of New York
333 Jay Street
Brooklyn, New York 11201

Professor K. Masubuchi
Massachusetts Institute of Technology
Department of Ocean Engineering
Cambridge, Massachusetts 02139

M
January 1979

SUPPLEMENTARY DISTRIBUTION LIST
(Continued)

Professor J. W. Morris, Jr.
University of California
College of Engineering
Berkeley, California 94720

Dr. Neil E. Paton
Rockwell International Science Center
1049 Camino Dos Rios
P. O. Box 1085
Thousand Oaks, California 91360

Mr. A. Pollack
Naval Ships Research & Development Center
Code 2821
Annapolis, Maryland 21402

Professor W. F. Savage
Rensselaer Polytechnic Institute
School of Engineering
Troy, New York 02181

Professor O. D. Sherby
Stanford University
Materials Sciences Division
Stanford, California 94300

Dr. G. Ecer
Westingnouse Electric Corporation
Research & Development Center
Pittsburgh, Pennsylvania 15235

Dr. E. A. Starke, Jr.
Georgia Institute of Technology
School of Chemical Engineering
Atlanta, Georgia 30332

Professor David Turnbull
Harvard University
Division of Engineering and
Applied Physics
Cambridge, Massachusetts 02138

Dr. F. E. Wawner
University of Virginia
School of Engineering and Applied
Science
Charlottesville, Virginia 22901

Dr. C. R. Whitsett
McDonnell Douglas Research
McDonnell Douglas Corporation
Saint Louis, Missouri 63166

Dr. J. C. Williams
Carnegie-Mellon University
Department of Metallurgy and
Materials Sciences
Schenley Park
Pittsburgh, Pennsylvania 15213

Professor H. G. F. Wilsdorf
University of Virginia
School of Engineering and Applied
Sciences
Charlottesville, Virginia 22903

Professor R. Mehrabian
University of Illinois at Urbana-
Champaign
144 Mechanical Engineering Building
Urbana, Illinois 61801

Dr. N. J. Grant
Massachusetts Institute of Technology
Department of Materials Science
and Engineering
Cambridge, Massachusetts 02139

Professor P. R. Strutt
University of Connecticut
School of Engineering
Department of Metallurgy
Storrs, Connecticut 06268

Mr. I. Caplan
David W. Taylor Naval Ship Research
and Development Center
Code 2813
Annapolis, Maryland 21402

Dr. B. R. Leverant
Southwest Research Institute
8500 Culebra Road
P. O. Box 28510
San Antonio, Texas 78284